Semiclassical theory of two-photon polarization-dependent fractional optical collisions: Application to the Mg-He($3s^2\,{}^1S_0 \rightarrow 3p\,{}^1P_1 \rightarrow 5s\,{}^1S_0,\ 4d\,{}^1D_2$) optical collision

D. V. Kupriyanov, I. M. Sokolov, A. V. Slavgorodskii, and A. I. Trubilko*
Department of Theoretical Physics, State Technical University, 195251 St. Petersburg, Russia
(Received 8 December 1998)

We have analyzed by perturbation theory technique two-photon polarization-dependent fractional optical collisions. In its general form the cross section of the collision is expressed as the overlap integral of its spectral profile with the spectrum of the second order correlation function of the electromagnetic field. Based on the semiclassical expansion of radial wave functions and of a retarded Green function we have expressed the spectral profile of the cross section in terms of well understood semiclassical characteristics of the process such as the rotational transformations of the transition dipole moments and the transition amplitudes describing the adiabatic or nonadiabatic dynamics of the electronic subsystem along classical trajectories. As a practical example, we have calculated the Mg-He ($3s^2\,{}^1S_0 \rightarrow 3p\,{}^1P_1 \rightarrow 5s\,{}^1S_0,\ 4d\,{}^1D_2$) fractional optical collision cross section. The partial wave analysis for excitation up to the $5s\,{}^1S_0$ state has shown the nonvalidity of quasistatic approximation based on successive single-photon transitions for some frequency detunings. For example, for the positive detuning from two-photon atomic resonance we have obtained the dominant contribution coming from the direct two-photon Franck-Condon transitions. Such a contribution gives the magnitude of the polarization ratio, characterizing the dependence of the cross section on mutual laser polarizations at the first and at the second steps of the photoexcitation, different than for successive single-photon Franck-Condon transitions. In the more complicated case of excitation up to the $4d\,{}^1D_2$ state of magnesium the role of the interference between different photoexcitation channels becomes important. The polarization ratio has a stable value close to $\frac{1}{7}$ in a broad spectral range in the blue wing of the second frequency detuning. There is a strong dependence of the polarization ratio in the red wing of the second detuning. Such spectral behavior can be explained by the partial selection in the red wing of the atomic resonance line, perturbed by the collisions of those Zeeman transitions in which contributions in the polarization ratio have different orders and different signs.
[S1050-2947(99)08308-0]

PACS number(s): 34.50.Rk, 34.80.Qb, 33.80.Gj

I. INTRODUCTION

The experiments on optical collisions are successfully used as a tool for the study of interatomic interactions and internal dynamics of atomic collisions [1–9]. The idea of the method is a probe by laser radiation of the diatomic system created in an atomic collision. The outgoing excited atomic fragments carrying the information about interrupted collision can be detected either directly in atomic beam experiments [7,9] or indirectly by measuring the atomic fluorescence in cell experiments [3–6,8]. In the latter case the transformation of exciting light into atomic fluorescence observed in the experiment is often called in literature collisional redistribution of light. Being an example of the continuum-continuum spectroscopy, the optical collision technique provides effective and sometimes the only accessible information when no transitions to bound states contribute in an absorption spectrum. The general problem in description of experimental results is that typically there are many optical transitions and decaying channels involved in the process, which can interfere and interact with one another. Therefore in practical realizations of the technique the additional polarization-dependent monitoring of optical collision is very useful because it often makes the spectral analysis more clear. By measuring the polarization dependence of far-wing absorption profiles we can better understand such polarization-sensitive characteristics of the process as the symmetry of the optical transitions and nonadiabatic dynamics.

In Refs. [10–12] the optical collision method was discussed in the more general case of two-photon collisional redistribution of radiation. The photoexcitation and the probe of a colliding pair by nonresonant photons under quasistatic (or close to quasistatic) conditions makes it possible to probe in experiment even a small segment of an atomic collision trajectory. The preliminary demonstration of such a promising experimental technique, named fractional optical collisions, was done recently in experiments [13] on magnesium–rare-gas partner optical collision. Because the photoabsorption spectra are usually presented as a function of two detunings between the photon frequencies and the resonance frequencies relating to the transitions into upper and intermediate atomic states, the spectral analysis of fractional optical collision is more complicated than in the single-photon case. The experimental data provided in the experiments [13] showed that in such a case the polarization-dependent monitoring is most helpful and informative in the analysis of the photoabsorption spectra.

There is another peculiarity of the two-photon optical collision technique connected with statistical properties of exciting light, which would be interesting to study in an experiment. For example, if there were mutual correlation in

*Present address: Department of Theoretical Physics and Astronomy, State Pedagogical University, 191187 St. Petersburg, Russia.

photon fluxes of both the exciting light beams, it would also lead to the correlation of photoabsorption events. Such external correlation could make it possible to observe the internal correlation of photoabsorption events directly connected with the dynamics of the fractional collision itself. In a simple case, in quasistatic conditions, it makes possible observation of the time delay in atomic motion between Condon points. We can point out here some analogy with an experimental technique commonly used in modern photochemistry and based on ultrashort laser pulses, which demonstrates the direct resolution and control of internal wave-packet dynamics in (steplike) photoexcitation of the molecules by time-delayed (-correlated) femtosecond laser pulses, see Refs. [14,15], and references therein.

In the present paper we are going to develop the theory of two-photon fractional optical collisions from two points of view. First, we are motivated to make a physically clear semiclassical analysis of two-photon polarization-dependent absorption based on second order of perturbation theory. The general expressions derived can be used for explanation of polarization-dependent spectra of optical collisions observed in experiments. We consider here the example of Mg-He fractional optical collision, because for such a pair the interaction potentials in the excited states can be calculated with better accuracy than for other rare-gas partners. Secondly, we are motivated to involve in our analysis the correlation properties of exciting light and we develop the theory valid for the light with arbitrary statistics, which can be either classical or nonclassical. It is important that in our discussion we treat in semiclassical approximation only the dynamics of an atomic subsystem, but we follow this with a complete quantum analysis in describing the electromagnetic field subsystem. The effects of mutual correlation connected with classical or quantum statistics of the excited light can be rather interesting for planning new experiments on two-photon fractional optical collisions.

The paper is organized as follows. In Sec. II we present general perturbation theory analysis of the diatomic density matrix based on Keldysh diagram technique. In Sec. III we derive the quantum and semiclassical expressions for the optical collision cross section. In Sec. IV we present the results of numerical calculations for Mg-He optical collisions. Section V is devoted to conclusions.

II. GENERAL ANALYSIS OF THE OPTICAL EXCITATION OF A DIATOMIC SYSTEM IN THE SECOND ORDER OF PERTURBATION THEORY

A. Diagram expansion for the diatomic density matrix

In this section we derive general expressions for the density matrix of a diatomic system produced by two-photon optical excitation of an arbitrary initial state. Our approach is based on the perturbation theory with a quantum description of exciting light valid for an arbitrary quantum state of an electromagnetic field. We point out that in nonlinear optical processes like two-photon absorption the quantum and classical descriptions of the light can lead to some difference in final results. To remove from our discussion possible inaccuracy coming from the classical description, our analysis is based on a general second quantized formalism. We adhere to a convenient diagram approach developed by Konstantinov and Perel in [16] and Keldysh in [17], see also [18], for arbitrary nonequilibrium many-particle quantum systems. In the Keldysh diagram formalism the density matrix of any particle (simple or compound) can be obtained through the perturbation theory expansion of the following Green function:

$$iG^{(-+)}_{ff'}(\mathbf{r}t;\mathbf{r}'t') = \pm\langle \Psi^{\dagger}_{f'}(\mathbf{r}'t')\Psi_{f}(\mathbf{r}t)\rangle, \tag{2.1}$$

where $\Psi_f(\ldots)$ and $\Psi^{\dagger}_{f'}(\ldots)$ are the space-time-dependent annihilation and creation operators of the particles in the Heisenberg representation. We denote as $\mathbf{r},\mathbf{r}'$ the center of mass coordinates and as f,f' the sets of internal quantum numbers of the particles. The angle brackets describe the averaging over the full initial density operator of the system. We assume that initially the density operator can be split as the product of the operators for different subsystems: particles, fields, etc. Then the single-particle density matrix can be obtained by taking the Green function (2.1) at coincident times as follows:

$$\rho_{ff'}(\mathbf{r},\mathbf{r}';t) = \pm iG^{(-+)}_{ff'}(\mathbf{r}t;\mathbf{r}'t). \tag{2.2}$$

The upper/lower signs in Eqs. (2.1),(2.2) relate to boson or fermion statistics, respectively.

Generalizing the approach of [16–18] we assume here that $\Psi,\Psi^{\dagger}$ operators can be treated as the second quantized operators of a compound diatomic system, i.e., quasimolecule. This means that we consider the gas medium where the active atoms (interacted with a field) are put in an environment of highly concentrated foreign gas. The energy structure of the active atoms is quasiresonant to the spectrum of optical excitation, but the interaction with foreign atoms is strong enough to perturb the energy levels of the active atom and it cannot be ignored in calculation of the photoabsorption spectrum. In such a case quantum numbers f,f' are associated with the full set of diatomic quantum numbers and in dependence on recoil energy they can related to either the bound or continuous spectrum of the system. Particularly in the optical collision case, when transitions are initiated between continuous spectra of both the lower and upper states, we apply the Green function formalism to the system where internal states are nonbound and quantum numbers f,f' are associated with the continuous spectrum of the quasimolecule. The presence of the quantum statistics permutation change of the sign in Eqs. (2.1),(2.2) is not really important if the diatomic gas has Boltzmann statistics.

Let us assume that initially all the atoms and quasimolecules are in the lower energy states described by the set of quantum numbers i and they can be excited in the upper states f by two-photon optical excitation only. We restrict ourselves by considering the interaction of the quasimolecule with the radiation in the dipole and rotating wave approximation when the interaction Hamiltonian in the interaction representation is given by

$$V(\mathbf{r},t) = -\sum_{ab} (d^{\nu})_{ba} E^{(+)}_{\nu}(\mathbf{r},t)\Psi^{(0)\dagger}_{b}(\mathbf{r},t)\Psi^{(0)}_{a}(\mathbf{r},t) + \text{H.c.}, \tag{2.3}$$

where $E^{(+)}_{\nu}(\ldots)$ is the positive frequency part of the νth

component of an electric field vector and $(d^{\nu})_{ba}$ is the transition dipole matrix element between any lower a and upper states b. We use here and throughout covariant notation for tensor indices because the difference between covariant and contravariant components can be important in the irreducible representation, see [19]. The Ψ operators with zero indices in Eq. (2.3) are associated with the interaction representation. The excited-state Green function appears in the second order of perturbation theory and it can be described by the following Keldysh-type diagram:

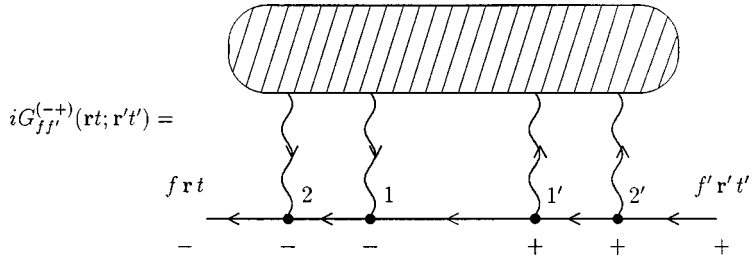

(2.4)

where we kept only the lowest order in the interaction of the quasimolecule with the electromagnetic field. Internal straight lines in this diagram are retarded and advanced diatomic Green functions describing the evolution of the system in an intermediate state. The waved lines and vertices are the photon propagation functions and interactions with the field, respectively. The dashed block in diagram (2.4) is the general second order correlation function of the electromagnetic field, which was introduced by Glauber [20], and its analytical definition will be given below in Eq. (2.6). We assume in diagram (2.4) the general quantum state of the light initiating the two-photon transitions.

Our analytical analysis of the diagram (2.4) is based on the following assumptions. First, it is convenient to make the calculation in the center of mass frame. This permits of the kinetic energy of the system after excitation because it is much less in order of magnitude than the rate of spontaneous decay. The latter characterizes the relaxation of excited and intermediate states and gives a natural scale for evaluating the integrals over internal time arguments. Secondly, we need to know the density matrix of the internal state of the diatomic system only, which is given by the integral

$$\rho_{ff'}(t)=\pm\int iG^{(-+)}_{ff'}(\mathbf{r}t;\mathbf{r}t)d^3r. \tag{2.5}$$

To evaluate this integral we assume that the second order electric field correlation function taken at coincident spatial points does not depend on spatial coordinates, i.e.,

$$\langle\tilde{T}[E^{(-)}_{\nu'_1}(\mathbf{r}t'_1)E^{(-)}_{\nu'_2}(\mathbf{r}t'_2)]T[E^{(+)}_{\nu_1}(\mathbf{r}t_1)E^{(+)}_{\nu_2}(\mathbf{r}t_2)]\rangle = D_{\nu_1\nu_2;\nu'_1\nu'_2}(t_1,t_2;t'_1,t'_2), \tag{2.6}$$

where T and $\tilde{T}$ are the time ordering and antiordering operators and $E^{(\pm)}_{\nu}(\ldots)$ are the positive and negative frequency components of the electric field. Physically this means spatial homogeneous excitation in an optically thin medium. Third, we assume that the exciting radiation is quasimonochromatic, so the integrals over t_1,t'_1 and t_2,t'_2 are determined mainly by the interaction with the modes near the average frequencies $\overline{\omega_1}$ and $\overline{\omega_2}$, respectively.

With such assumptions we obtain the following expression for the density matrix of the internal state:

$$\begin{aligned}\rho_{ff'}(t)=&\sum_{ii'}\sum_{rr'}\int\int\int\int dt_1dt_2dt'_1dt'_2\\
&\times\exp\left(-\frac{i}{\hbar}\epsilon_f(t-t_2)-\frac{1}{2}\gamma_f(t-t_2)-\frac{i}{\hbar}\epsilon_r(t_2-t_1)-\frac{1}{2}\gamma_r(t_2-t_1)-\frac{i}{\hbar}\epsilon_it_1\right)\\
&\times\exp\left(\frac{i}{\hbar}\epsilon_{f'}(t-t'_2)-\frac{1}{2}\gamma_{f'}(t-t'_2)+\frac{i}{\hbar}\epsilon_{r'}(t'_2-t'_1)-\frac{1}{2}\gamma_{r'}(t'_2-t'_1)+\frac{i}{\hbar}\epsilon_{i'}t'_1\right)\\
&\times\theta(t-t_2)\theta(t_2-t_1)\theta(t-t'_2)\theta(t'_2-t'_1)\rho_{ii'}\\
&\times\left(\frac{i}{\hbar}\right)^2(d^{\nu_2})_{fr}(d^{\nu_1})_{ri}\left(-\frac{i}{\hbar}\right)^2(d^{\nu'_2})_{r'f'}(d^{\nu'_1})_{i'r'}D_{\nu_1\nu_2;\nu'_1\nu'_2}(t_1,t_2;t'_1,t'_2),\end{aligned} \tag{2.7}$$

where $\epsilon_i, \epsilon_f, \epsilon_r$ are the internal energies for initial (i) and final (f), and intermediate (r) states, respectively; γ_f, γ_r are the rates of spontaneous decays of excited states; and $\rho_{ii'}$ is the initial density matrix of the quasimolecule. The step function $\theta(\tau)$ is equal to 1 or 0 for $\tau>0$ or $\tau<0$, respectively.

B. Generalized distorted-wave approximation

The derived expression (2.7) shows the relationship between initial and excited density matrices for weak exciting light existing in an arbitrary quantum state. But such a general expression is still formal as long as it does not specify the basis sets for initial and excited states. Moreover, considered at arbitrary time arguments and in non-steady-state conditions, it is too general and contains many details which can be unimportant for real experimental situations. Therefore it is convenient to transform Eq. (2.7) to a less general but clearer form of the collisional cross section where optical excitation plays the role of a small perturbation interacted with the system during the collision. In quantum scattering theory such an approach is known as the distorted-wave approximation and it was introduced in optical collision theory by Julienne and co-workers in [21,22] in the example of a single-photon optical collision.

Let us define the density matrix in a coordinate representation by the following transformation:

$$\rho(\mathbf{R},q;\mathbf{R}',q';t)=\sum_{ff'} \Psi_f(\mathbf{R},q)\rho_{ff'}(t)\Psi^*_{f'}(\mathbf{R}',q'), \tag{2.8}$$

where we choose as f representation the basis of outgoing wave functions determined by the following boundary condition:

$$\Psi_f(\mathbf{R},q)\equiv\Psi^{(-)}_{\mathbf{k}\mu}(\mathbf{R},q)\rightarrow e^{i\mathbf{k}\cdot\mathbf{R}}\psi_\mu(q) + \sum_{\bar{\mu}} \frac{1}{R} e^{-i\bar{k}R} f^{(-)}_{\bar{\mu}\mu}(\bar{\mathbf{k}},\mathbf{k})\psi_{\bar{\mu}}(q). \tag{2.9}$$

Here $\mathbf{R}$ is the radius vector of the internuclear axis and q denotes the set of all electronic (including spin) coordinates. The wave function $\psi_\mu(q)$ is the atomic wave function of a free atom. We consider here the case when the foreign atom is in the ground state with the $^1S_0$ configuration conserved during the collision. To simplify notation here and throughout, in the set of atomic quantum numbers we show only the angular momentum projection μ and omit the angular momentum j as well as other quantum numbers whenever possible. However, we note that the internal atomic states can be characterized by the quantum numbers relating to different recoil energies, so the incoming wave number $\bar{k}$ in scattering amplitude $f^{(-)}_{\mu\mu}(\bar{\mathbf{k}},\mathbf{k})$ can differ from the outgoing wave number k.

Based on the coordinate representation of the density matrix (2.8) we can introduce the probability flux of outgoing particles as follows:

$$\mathbf{j}(q,q';\mathbf{R},t)=\frac{i\hbar}{2m}[\nabla_{\mathbf{R}'}\rho(\mathbf{R},q;\mathbf{R}',q';t) - \nabla_{\mathbf{R}}\rho(\mathbf{R},q;\mathbf{R}',q';t)]\Big|_{\mathbf{R}'=\mathbf{R}}. \tag{2.10}$$

The differential cross section in the center-of-mass frame can be associated with this flux propagating in an arbitrary direction taken at asymptote $R,t\rightarrow\infty$ and normalized to the incident flux of incoming particles. In such a procedure we ignore radiative decay of upper and intermediate excited states and substitute γ_f and γ_r by $+0$. It seems reasonable because the scattering asymptote of the wave packet, described by density matrix (2.7), conserves its shape as long as the excited quasimolecule disappears as a result of spontaneous decay. However, it is important to save the decay constants as $+0$ for the intermediate state because they show correct analytical behavior of the energy denominators in the vicinities of the resonance energy. We should point out here that such an approximation restricts our discussion and does not allow consideration of the cases of resonances relating to pure single- or two-photon absorption by free atoms.

As the basis set of initial states i we use the set of incoming wave functions determined by the following boundary condition:

$$\Psi_i(\mathbf{R},q)\equiv\Psi^{(+)}_{\mathbf{k}_0\mu_0}(\mathbf{R},q)\rightarrow e^{i\mathbf{k}_0\cdot\mathbf{R}}\psi_{\mu_0}(q) + \sum_{\bar{\mu}_0} \frac{1}{R} e^{i\bar{k}_0R} f^{(+)}_{\bar{\mu}_0\mu_0}(\bar{\mathbf{k}}_0,\mathbf{k}_0)\psi_{\bar{\mu}_0}(q). \tag{2.11}$$

Such a basis set is most suitable to define the probability flux of colliding atoms. For unit normalization volume the probability flux is given by $\hbar\mathbf{k}_0/m$, where m is the reduced atomic mass.

Substituting wave functions (2.9),(2.11) into (2.8),(2.10) and making typical scattering theory approximations with respect to the asimptotic behavior of the wave packet, we obtain the following expression for the differential cross section of the optical collision:

$$\frac{d\sigma_{\mu\mu'}}{d\Omega_{\mathbf{k}}}=\int\int\int\int \frac{d\omega_1}{2\pi}\frac{d\omega_2}{2\pi}\frac{d\omega'_1}{2\pi}\frac{d\omega'_2}{2\pi} \times D_{\nu_1\nu_2;\nu'_1\nu'_2}(\omega_1,\omega_2;\omega'_1,\omega'_2)\sum_{\mu_0\mu'_0}\frac{1}{(2\pi)^2}\frac{m^2k}{\hbar^4k_0} \times\langle\Psi^{(-)}_{\mathbf{k}\mu}|d^{\nu_2}G^{(+)}(\epsilon_{\mu_0}(k_0)+\hbar\omega_1)d^{\nu_1}|\Psi^{(+)}_{\mathbf{k}_0\mu_0}\rangle\rho_{\mu_0\mu'_0} \times\langle\Psi^{(+)}_{\mathbf{k}_0\mu'_0}|d^{\nu'_1}G^{(-)}(\epsilon_{\mu'_0}(k_0)+\hbar\omega'_1)d^{\nu'_2}|\Psi^{(-)}_{\mathbf{k}\mu'}\rangle. \tag{2.12}$$

The differential cross section describes the formation of the excited atoms outgoing in the direction of solid angle $\Omega_{\mathbf{k}}$ and characterized by the coherence between μ,μ' atomic states. The solid angle in Eq. (2.12) characterizes the direction of the outgoing wave vector $\mathbf{k}$ in the reference frame with the z

axis along incoming wave vector $\mathbf{k}_0$. The evolution of the system in an intermediate state is described by retarded and advanced Green operators $G^{(+)}(\epsilon)$ and $G^{(-)}(\epsilon)$ which are given by

$$G^{(\pm)}(\epsilon)=\frac{1}{\epsilon-H\pm i0}, \tag{2.13}$$

where H is the Hamiltonian of the diatomic system and the arguments of the Green operators in Eq. (2.12) are the virtual energies of the intermediate state. The polarization state of the atom before the collision is described by its polarization density matrix $\rho_{\mu_0\mu_0'}$.

As follows from Eq. (2.12) the light correlation function appears as a Fourier expansion

$$D_{\nu_1\nu_2;\nu_1'\nu_2'}(\omega_1,\omega_2;\omega_1',\omega_2')=\int\int\int\int dt_1dt_2dt_1'dt_2' \exp(i\omega_1t_1+i\omega_2t_2-i\omega_1't_1'-i\omega_2't_2') \times D_{\nu_1\nu_2;\nu_1'\nu_2'}(t_1,t_2;t_1',t_2') \tag{2.14}$$

defined for $\omega_1,\omega_2,\omega_1',\omega_2'>0$. We note also that the expression for the differential cross section in the form (2.12) can be derived under the assumption of a stationary light source when $\omega_1+\omega_2=\omega_1'+\omega_2'$. In such a case the energies of excited atoms $\epsilon_\mu(k)=\epsilon_{\mu_0}(k_0)+\hbar(\omega_1+\omega_2)$ and $\epsilon_{\mu'}(k)=\epsilon_{\mu_0'}(k_0)+\hbar(\omega_1'+\omega_2')$ are equal, $\epsilon_\mu(k)=\epsilon_{\mu'}(k)$ and $k'=k$, because the Zeeman states μ,μ' belong to the same degenerate atomic level. Otherwise, for a general light source, it is possible to produce coherence not only between Zeeman states but also between outgoing wave numbers k,k'. We restrict the possible view of the light correlation function by a stationary approximation in this paper. From a practical point of view, it means that the excitation is initiated by cw light sources or pulsed lasers with pulse duration much longer than a typical collisional time.

The above analysis shows that, as in other two-photon processes, in the optical collision case the electromagnetic field of the exciting light governs the process by its general second order correlation function. Such a type of correlation functions emphasizing the quantum nature of light appears in different applications of modern quantum optics: in the study of light statistics, correlation phenomena and high order interference. If noncommutation of the operators or quantum behavior of the electric field fluctuations are important for the light statistics, the quantum nature of light can manifest itself in the excitations initiated by two-photon optical collisions. However, in the existing experiments the two-photon transitions in the collisional domain were initiated by the radiation coming from two independent noncorrelated laser sources [13]. In such a case there is no difference between a quantum and classical description, because the second order correlation function is factorized as a product of two first order correlation functions relating to the independent laser sources.

III. OPTICAL COLLISION CROSS SECTION

A. Quantum-mechanical analysis

The incoming and outgoing wave functions (2.11), (2.9) defined in a laboratory frame can be transformed to the R-helicity basis set as follows:

$$\Psi^{(+)}_{\mathbf{k}_0\mu_0}(\mathbf{R},q)=\sum_{\Omega_0}(-)^{-j_0}D^{j_0*}_{\mu_0-\Omega_0}(\alpha_0,\beta_0,0)\Psi^{(+)}_{\mathbf{k}_0\Omega_0}(\mathbf{R},q),$$
$$\Psi^{(-)}_{\mathbf{k}\mu}(\mathbf{R},q)=\sum_{\Omega}D^{j*}_{\mu\Omega}(\alpha,\beta,0)\Psi^{(-)}_{\mathbf{k}\Omega}(\mathbf{R},q). \tag{3.1}$$

Here Ω_0 and Ω are the angular-momentum projections on the directions $-\mathbf{k}_0$ and $\mathbf{k}$, respectively. We call such projections of angular-momentum R-helicity, because in a classical picture of the collision the vector $\mathbf{R}$ rotates in space between two ''in'' and ''out'' asymptotes of a classical trajectory. Since in the adiabatic approximation the internal angular-momentum projection on $\mathbf{R}$ direction is conserved, an R-helicity representation is more suitable as a basis for the scattering wave functions; see [23,24]. The transformations between laboratory and helicity frames are described by Wigner D functions $D^{j_0}_{\mu_0-\Omega_0}(\alpha_0,\beta_0,0)$ and $D^{j}_{\mu\Omega}(\alpha,\beta,0)$ depending on angles, which characterize the directions of $\mathbf{k}_0$ and $\mathbf{k}$ in an arbitrary laboratory frame. We use here and throughout the definition of the D function as in Ref. [19].

Instead of Zeeman coherences, the atomic polarization is better described in terms of irreducible tensor components, see [25,26,19]. The formation of a KQ irreducible component (defined in covariant form [27]) in the collision is described by the following cross section;

$$\frac{d\sigma_{KQ}}{d\Omega}=\sum_{\mu\mu'}\left(\frac{2K+1}{2j+1}\right)^{1/2}C^{j\mu'}_{j\mu KQ}\frac{d\sigma_{\mu\mu'}}{d\Omega}, \tag{3.2}$$

where j is an angular momentum of the outgoing atom and $C^{\cdots}_{\cdots\cdots}$ are the Clebsch-Gordan coefficients in the notation of Ref. [19]. In the same way we can expand the density matrix of the incoming atom in terms of κq irreducible components as follows;

$$\rho_{\mu_0\mu_0'}=\sum_{\kappa q}\left(\frac{2\kappa+1}{2j_0+1}\right)^{1/2}C^{j_0\mu_0'}_{j_0\mu_0\kappa q}\rho_{\kappa q}(j_0), \tag{3.3}$$

where j_0 is the angular momentum of the incoming atom.

The polarization structure of electric field correlation function (2.6), (2.14) is given by

$$D_{\nu_1\nu_2;\nu_1'\nu_2'}(\omega_1,\omega_2;\omega_1',\omega_2')=(\mathbf{e}_1)_{\nu_1}(\mathbf{e}_2)_{\nu_2}(\mathbf{e}_1^*)_{\nu_1'}(\mathbf{e}_2^*)_{\nu_2'}\times\tilde{D}(\omega_1,\omega_2;\omega_1',\omega_2'), \quad (3.4)$$

where $\mathbf{e}_1,\mathbf{e}_2$ are the polarization vectors of the light in the vicinities of the average frequencies $\overline{\omega_1}$ and $\overline{\omega_2}$, i.e., at the first and at the second steps of the excitation, respectively. Then we can express the differential cross section (3.2) in the following form:

$$\frac{d\sigma_{KQ}}{d\Omega_{\mathbf{k}}}=\int\int\int\int\frac{d\omega_1}{2\pi}\frac{d\omega_2}{2\pi}\frac{d\omega_1'}{2\pi}\frac{d\omega_2'}{2\pi}\tilde{D}(\omega_1,\omega_2;\omega_1',\omega_2')\times\frac{d\tilde{\sigma}_{KQ}}{d\Omega_{\mathbf{k}}}(\omega_1,\omega_2;\omega_1',\omega_2'), \quad (3.5)$$

where we introduced the following spectral profile of the cross section:

$$\frac{d\tilde{\sigma}_{KQ}}{d\Omega_{\mathbf{k}}}(\omega_1,\omega_2;\omega_1',\omega_2')=\frac{1}{(2\pi)^2}\frac{m^2k}{\hbar^4k_0}\sum_{\Omega_0\Omega_0'}\sum_{\Omega\Omega'}\sum_{\kappa q}\rho_{\kappa q}(j_0)(-)^{j-\Omega+j_0+\Omega_0}C^{K(\Omega'-\Omega)}_{j\Omega' j-\Omega}\times C^{\kappa(\Omega_0-\Omega_0')}_{j_0-\Omega_0' j_0\Omega_0}D^{K*}_{Q\Omega'-\Omega}(\alpha,\beta,0)D^{\kappa*}_{q\Omega_0-\Omega_0'}(\alpha_0,\beta_0,0)\times\langle\Psi^{(-)}_{\mathbf{k}\Omega}|(\mathbf{de}_2)G^{(+)}(\epsilon_0(k_0)+\hbar\omega_1)(\mathbf{de}_1)|\Psi^{(+)}_{\mathbf{k}_0\Omega_0}\rangle\times\langle\Psi^{(-)}_{\mathbf{k}\Omega'}|(\mathbf{de}_2)G^{(+)}(\epsilon_0(k_0)+\hbar\omega_1')(\mathbf{de}_1)|\Psi^{(+)}_{\mathbf{k}_0\Omega_0'}\rangle^*. \quad (3.6)$$

Here we used the relationship between Green operators $G^{(-)}(\epsilon)=G^{(+)\dagger}(\epsilon)$ and assumed that all the Zeeman states Ω_0,Ω_0' have the same energy denoted as ϵ_0. Let us note that the spectral profile (3.6) does not have the dimensions of a cross section. We mark here and throughout by an additional tilde sign the observables, which can be interpreted as cross sections after evaluating the overlap integral with the correlation function, see Eq. (3.5), and we will call them cross sections in those cases where no confusion can arise.

It is useful to expand the wave functions $\Psi^{(\pm)}$ and Green function $G^{(+)}$ in the basis set of adiabatic wave functions with definite total angular momentum. Such partial wave expansions of the wave functions are given by

$$\Psi^{(+)}_{\mathbf{k}_0\Omega_0}(\mathbf{R},q)=\frac{1}{R}\sum_{\overline{\Omega}_0}\sum_{J_0M_0}(2J_0+1)\times D^{J_0*}_{M_0\overline{\Omega}_0}(\alpha_{\mathbf{R}},\beta_{\mathbf{R}},0)D^{J_0}_{M_0-\Omega_0}(\alpha_0,\beta_0,0)\times e^{i\pi J_0/2}v^{(+)J_0}_{\overline{\Omega}_0\Omega_0}(R)\phi_{\overline{\Omega}_0}(R,q),$$
$$\Psi^{(-)}_{\mathbf{k}\Omega}(\mathbf{R},q)=\frac{1}{R}\sum_{\overline{\Omega}}\sum_{JM}(2J+1)D^{J*}_{M\overline{\Omega}}(\alpha_{\mathbf{R}},\beta_{\mathbf{R}},0)\times D^{J}_{M\Omega}(\alpha,\beta,0)e^{i\pi J/2}v^{(-)J}_{\overline{\Omega}\Omega}(R)\phi_{\overline{\Omega}}(R,q), \quad (3.7)$$

where $\phi_{\overline{\Omega}_0}(R,q)$ and $\phi_{\overline{\Omega}}(R,q)$ are the electronic adiabatic wave functions of lower and upper states of the quasimolecule, respectively. To simplify notation here and throughout, wherever possible, we specify the quantum state of the quasimolecule by the electronic angular momentum projections on the internuclear direction $\overline{\Omega}_0$ and $\overline{\Omega}$ and omit other quantum numbers. The angles $\alpha_{\mathbf{R}}$ and $\beta_{\mathbf{R}}$ characterize the direction of $\mathbf{R}$ in a laboratory frame. The radial wave functions $v^{(+)J_0}_{\overline{\Omega}_0\Omega_0}(R)$ and $v^{(-)J}_{\overline{\Omega}\Omega}(R)$ can be found as the solution of the scattering equations in the molecular basis set, see Refs. [23, 24], with the following boundary conditions:

$$v^{(+)J_0}_{\overline{\Omega}_0\Omega_0}(R)\to\frac{i}{2(\overline{k}_0k_0)^{1/2}}[\delta_{\overline{\Omega}_0\Omega_0}e^{-ik_0R+i\pi J_0/2}-e^{ik_0R-i\pi J_0/2}S^{(+)J_0}_{\overline{\Omega}_0\Omega_0}(\overline{k}_0,k_0)],$$
$$v^{(-)J}_{\overline{\Omega}\Omega}(R)\to-\frac{i}{2(\overline{k}k)^{1/2}}[\delta_{\overline{\Omega}\Omega}e^{ikR-i\pi J/2}-e^{-ikR+i\pi J/2}S^{(-)J}_{\overline{\Omega}\Omega}(\overline{k},k)] \quad (3.8)$$

at $R\to\infty$. For the Green function [kernel of Green operator $G^{(+)}(\epsilon)$] the similar expansion is given by

$$G^{(+)}(\mathbf{R}_2,q_2;\mathbf{R}_1,q_1)=\frac{1}{4\pi R_2R_1}\sum_{\Omega_2\Omega_1}\times\sum_{J_1M_1}(2J_1+1)D^{J_1*}_{M_1\Omega_2}(\alpha_2,\beta_2,0)\times D^{J_1}_{M_1\Omega_1}(\alpha_1,\beta_1,0)G^{J_1}_{\Omega_2\Omega_1}(R_2,R_1)\times\phi_{\Omega_2}(R_2,q_2)\phi^*_{\Omega_1}(R_1,q_1), \quad (3.9)$$

where angles α_1,β_1 and α_2,β_2 show the directions of the vectors $\mathbf{R}_1$ and $\mathbf{R}_2$, respectively. The radial Green function $G^{J_1}_{\Omega_2\Omega_1}(R_2,R_1)$ can be found as the solution of the system of the radial scattering equations for the energy ϵ with the following boundary conditions:

$$G^{J_1}_{\Omega_2\Omega_1}(R_2,R_1)\to\frac{im}{\hbar^2(k_2k_1)^{1/2}}[S^{(+)J_1}_{\Omega_2\Omega_1}(k_2,k_1)e^{ik_2R_2+ik_1R_1-i\pi J_1}-\delta_{\Omega_2\Omega_1}e^{ik_1(R_>-R_<)}] \tag{3.10}$$

at R_2, $R_1\to\infty$ where we denoted $R_>=\max\{R_2,R_1\}$ and $R_<=\min\{R_2,R_1\}$.

The expansions (3.7),(3.9) are very convenient for the analysis of the slow atomic collisions at broad range of recoil energies. As long as an adiabatic approximation is valid in an interaction region the Green function is simply diagonal and $\Omega_2=\Omega_1$. The nonadiabatic effects initiating the transitions between different molecular states take place in the domains located near the vicinities of the crossing or anticrossing points of the potential curves of the molecule. The rotational nonadiabatic coupling is particularly important at large internuclear separations. The nonadiabatic transition amplitudes can be calculated by solving the scattering equations for the radial wave functions and the Green function in such domains. There are many model approximations to solve the nonadiabatic problem and it is often possible to find even the analytical solution of scattering equations. General discussion of the problem can be found in many reviews, see, for instance, [23], and references therein. In Appendix A we derive the expansion of Green function (3.9) and show the procedure of semiclassical solution of the scattering equations for this example.

By substituting the wave functions and the Green function in the form (3.7),(3.9) into Eq. (3.6) we could obtain a general partial expansion for the spectral profile of the differential cross section describing the formation of arbitrary polarization for the excited atom outgoing in an arbitrary direction. However, in the present paper we restrict ourselves to the analysis of a simple but most practically important situation, when only the total population of outgoing fragments in the optical collisions of initially nonpolarized atoms is detected. Such a situation corresponds to a commonly used experimental detection scheme, one which we are going to discuss. Also it lets us simplify the analysis of the excitation channels and interference effects as well as their dependence on mutual orientation of polarization vectors $\mathbf{e}_1$ and $\mathbf{e}_2$ of the first and the second lasers.

By averaging the differential cross section (3.6) over the initial and final directions of the wave vectors and by substituting expansions (3.7),(3.9) we can express the spectral profile of the total cross section in the following form:

$$\begin{aligned}\tilde{\sigma}(\omega_1,\omega_2;\omega_1',\omega_2')&\equiv\frac{1}{4\pi}\int d\Omega_{\mathbf{k}}\int d\Omega_{\mathbf{k}_0}\\&\quad\times\sqrt{2j+1}\frac{d\tilde{\sigma}_{00}}{d\Omega_{\mathbf{k}}}(\omega_1,\omega_2;\omega_1',\omega_2')\\&=\sum_{X\Xi}(-)^{X+\Xi}\Phi_{X\Xi}(\mathbf{e}_1)\Phi_{X-\Xi}(\mathbf{e}_2)\\&\quad\times\tilde{Q}^{(X)}(\omega_1,\omega_2;\omega_1',\omega_2'),\end{aligned} \tag{3.11}$$

where we introduced the irreducible components for the light density matrix,

$$\begin{aligned}\Phi_{X\Xi}(\mathbf{e})&=-\sum_{\nu,\nu'}C^{X\Xi}_{1\nu'1\nu}(\mathbf{e}^*)_{\nu'}e_\nu\\&=\sum_{\nu,\nu'}(-1)^{1+\nu'}C^{X\Xi}_{1\nu'1\nu}e^*_{-\nu'}e_\nu\end{aligned} \tag{3.12}$$

for both polarization vectors $\mathbf{e}_1$ and $\mathbf{e}_2$. Expression (3.11) shows that the total cross section is formed from the tensor product of the light irreducible components of the first and the second laser weighted with the collisional factor $\tilde{Q}^{(X)}(\omega_1,\omega_2;\omega_1',\omega_2')$ depending on tensor rank. The weighting factor is given by

$$\begin{aligned}\tilde{Q}^{(X)}(\omega_1,\omega_2;\omega_1',\omega_2')&=\frac{16\pi m^2k}{\hbar^4k_0}\frac{1}{2j_0+1}\sum_{\bar{\Omega}}\sum_{\bar{\Omega}_0}\sum_{\bar{\Omega}\bar{\Omega}'}\sum_{\bar{\Omega}_0\bar{\Omega}_0'}\sum_{\Omega_1\Omega_1'}\sum_{\Omega_2\Omega_2'}\sum_{J}\sum_{J_0}\sum_{J_1,J_1'}(-)^{J_1+J_1'+J+J_0}\\&\quad\times(2J_0+1)[(2J_1+1)(2J_1'+1)]^{1/2}\begin{Bmatrix}1&1&X\\J_1'&J_1&J\end{Bmatrix}\begin{Bmatrix}1&1&X\\J_1'&J_1&J_0\end{Bmatrix}\\&\quad\times C^{J\bar{\Omega}}_{J_1\Omega_2 1\bar{\nu}_2}C^{J_1\Omega_1}_{J_0\bar{\Omega}_0 1\bar{\nu}_1}C^{J\bar{\Omega}'}_{J_1'\Omega_2' 1\bar{\nu}_2'}C^{J_1'\Omega_1'}_{J_0\bar{\Omega}_0' 1\bar{\nu}_1'}\mathcal{F}^{J_0J_1J}_{\Omega_0\bar{\Omega}_0\Omega_1\Omega_2\bar{\Omega}\Omega}(\omega_1,\omega_2)\mathcal{F}^{J_0J_1'J*}_{\Omega_0\bar{\Omega}_0'\Omega_1'\Omega_2'\bar{\Omega}'\Omega}(\omega_1',\omega_2'),\end{aligned} \tag{3.13}$$

where $\overline{\nu}_1=\Omega_1-\overline{\Omega}_0$, $\overline{\nu}_1'=\Omega_1'-\overline{\Omega}_0'$, $\overline{\nu}_2=\overline{\Omega}-\Omega_2$, and $\overline{\nu}_2'=\overline{\Omega}'-\Omega_2'$ are the vector indices of the transition dipole moments characterizing the changes of the electronic angular momentum from lower to intermediate and upper states. The transition overlap integral depending on the full set of initial and intermediate quantum numbers is given by

$$\mathcal{F}^{J_0J_1J}_{\Omega_0\overline{\Omega}_0\Omega_1\Omega_2\overline{\Omega}\Omega}(\omega_1,\omega_2)=\int_0^\infty dR_1\int_0^\infty dR_2 v^{(-)J*}_{\overline{\Omega}\Omega}(R_2)\times(d^-_{\overline{\nu}_2})_{\overline{\Omega}\Omega_2}G^{J_1}_{\Omega_2\Omega_1}(R_2,R_1)\times(d^-_{\overline{\nu}_1})_{\Omega_1\overline{\Omega}_0}v^{(+)J_0}_{\overline{\Omega}_0\Omega_0}(R_1), \tag{3.14}$$

where $(d^-_{\overline{\nu}_1})_{\Omega_1\overline{\Omega}_0}$ and $(d^-_{\overline{\nu}_2})_{\overline{\Omega}\Omega_2}$ are the transition dipole matrix elements defined in the body fixed frame and calculated between adiabatic electronic states at the inter nuclear separations R_1 and R_2, respectively. The dependence on photon frequencies ω_1 and ω_2 appears in Eq. (3.14) from the energy dependence of the Green function of the intermediate state and of the wave function of the upper state.

B. Semiclassical approximation

The derived expressions (3.11),(3.13) are restricted only by the approximations of perturbation theory and they can be used for numerical calculation directly. In such a procedure the wave functions and Green function should be considered as the exact solutions of quantum scattering equations. However, the nuclear motion of the atoms is mainly described by classical mechanics that makes it possible to simplify the analysis by introducing a semiclassical approximation for the radial wave functions. The global advantage of a semiclassical approach is in its clear physical sense and in the visual representation of the wave functions and the Green function. It is also important that for typical experimental conditions, when the recoil energy is close to room temperature, a semiclassical approximation has very good accuracy for comparison with experimental data. We expect that all the important physical effects will be well described by such an approximation.

In a semiclassical approximation the radial wave function at all internuclear separations can be presented as the sum of two waves, namely, ''in'' and ''out.'' The waves ''in'' and ''out,'' being the running waves inside and outside of the interaction region, exist for each incoming and outgoing radial wave functions. Let us emphasize that the terms ''incoming'' and ''in'' or ''outgoing'' and ''out'' have different physical meanings and they are not to be confused. The transformation from ''in'' to ''out'' waves takes place at the turning points or near the regions of classically forbidden motions. For simplicity we will assume that nonadiabatic and classical forbidden regions are separated so the calculation of nonadiabatic transition amplitudes and the transformations from ''in'' to ''out'' waves can be made independently. In such conditions the semiclassical approximation can be introduced by the following expansion of the radial wave functions:

$$v^{(+)J_0}_{\overline{\Omega}_0\Omega_0}(R)=\sum_{l_0}{}'\frac{i}{2\sqrt{k_0}}e^{i\delta^{J_0}_{l_0}(k_0,-)}\times\left\{\frac{1}{[k^{J_0}_{l_0}(R,-)]^{1/2}}a^{J_0}_{l_0}(R,-)e^{-i\mathcal{S}^{J_0}_{l_0}(R,-)-i\pi/4}-\frac{1}{[k^{J_0}_{l_0}(R,+)]^{1/2}}a^{J_0}_{l_0}(R,+)e^{i\mathcal{S}^{J_0}_{l_0}(R,+)+i\pi/4}\right\},$$

$$v^{(-)J}_{\overline{\Omega}\Omega}(R)=\sum_{l}{}'\frac{i}{2\sqrt{k}}e^{-i\delta^{J}_{l}(k,+)}\times\left\{\frac{1}{[k^{J}_{l}(R,-)]^{1/2}}b^{J}_{l}(R,-)e^{-i\mathcal{S}^{J}_{l}(R,-)-i\pi/4}-\frac{1}{[k^{J}_{l}(R,+)]^{1/2}}b^{J}_{l}(R,+)e^{i\mathcal{S}^{J}_{l}(R,+)+i\pi/4}\right\}. \tag{3.15}$$

Here we introduced ''path'' indices l_0 and l, which are the sequences of quantum states $\overline{\Omega}_0\ldots\Omega_0$ and $\overline{\Omega}\ldots\Omega$, respectively, which are passed by the atoms during the collision. The dots here denote the quantum numbers of all the intermediate states. The transitions between adiabatic states are caused by the nonadiabatic dynamics and the transformation from ''in'' to ''out'' waves takes place at the turning points or near the classical violation regions. We can say that indices l_0 and l show the possible paths coupling the states $\overline{\Omega}_0$ with Ω_0 and $\overline{\Omega}$ with Ω and the prime superscripts at sum signs in Eq. (3.15) show that all the paths with fixed initial state Ω_0 (for incoming wave function) or final state Ω (for outgoing wave function) make the contribution in those sums. The wave numbers, dependent on R, defined for ''in'' (with $-$ sign) and for ''out'' (with $+$ sign) parts of the trajectory, are given by

$$k^{J_0}_{l_0}(R,\pm)=\frac{1}{\hbar}\left[2m\left(E-U_{l_0}(R,\pm)-\frac{\hbar^2(J_0+\frac{1}{2})^2}{2mR^2}\right)\right]^{1/2}, \tag{3.16}$$

$$k^{J}_{l}(R,\pm)=\frac{1}{\hbar}\left[2m\left(E-U_{l}(R,\pm)-\frac{\hbar^2(J+\frac{1}{2})^2}{2mR^2}\right)\right]^{1/2}$$

and the action integrals and phase shifts are given by

$$\mathcal{S}^{J_0}_{l_0}(R,\pm)=\int_{R_{l_0}}^{R}k^{J_0}_{l_0}(R,\pm)dR, \tag{3.17}$$

$$\delta^{J_0}_{l_0}(k_0,-)=\lim_{R\to\infty}\left[\int_{R_{l_0}}^{R}k^{J_0}_{l_0}(R,-)dR-k_0R+\frac{\pi}{2}\left(J_0+\frac{1}{2}\right)\right],$$

$$\mathcal{S}^{J}_{l}(R,\pm)=\int_{R_l}^{R}k^{J}_{l}(R,\pm)dR,$$

$$\delta^{J}_{l}(k,+)=\lim_{R\to\infty}\left[\int_{R_l}^{R}k^{J}_{l}(R,+)dR-kR+\frac{\pi}{2}\left(J+\frac{1}{2}\right)\right],$$

where R_{l_0} and R_l are the coordinates of the turning points which depend on ''path'' quantum numbers. The ''path'' potentials are defined as $U_{l_0}(R,\pm)=U_{\bar{\Omega}_0}(R),\ldots,U_{\Omega_0}(R)$, $U_l(R,\pm)=U_{\Omega}(R),\ldots,U_{\bar{\Omega}}(R)$ where the choice of adiabatic potential is determined by the location of R in the path l_0 or l. The amplitudes $a_{l_0}^{J_0}(R,\pm)$ and $b_l^J(R,\pm)$, slowly varying on R, J, and on E (not shown here), are defined as a solution of the scattering equations in semiclassical form. For details of the derivation of the semiclassical representations (3.15) we refer the reader to Appendix B of [24].

For a radial Green function the semiclassical representation is derived in Appendix A. Finally we obtain

$$G_{\Omega_2\Omega_1}^{J_1}(R_2,R_1)=\sum_{l_1}{}'\left\{\frac{im}{\hbar^2[k_{l_1}^{J_1}(R_2,+)k_{l_1}^{J_1}(R_1,-)]^{1/2}}g_{l_1}^{J_1}(R_2,R_1;+-)e^{i\mathcal{S}_{l_1}^{J_1}(R_2,R_1;+-)+i\pi/2}\right.$$
$$-\frac{im}{\hbar^2[k_{l_1}^{J_1}(R_2,-)k_{l_1}^{J_1}(R_1,-)]^{1/2}}g_{l_1}^{J_1}(R_2,R_1;-)e^{i\mathcal{S}_{l_1}^{J_1}(R_2,R_1;-)+i\pi/2}\theta(R_1-R_2)$$
$$\left.-\frac{im}{\hbar^2[k_{l_1}^{J_1}(R_2,+)k_{l_1}^{J_1}(R_1,+)]^{1/2}}g_{l_1}^{J_1}(R_2,R_1;+)e^{i\mathcal{S}_{l_1}^{J_1}(R_2,R_1;+)+i\pi/2}\theta(R_2-R_1)\right\}. \tag{3.18}$$

Let us interpret the terms contributing to the right side of this expression. The second and the third terms describe the evolution of the electronic subsystem from point R_1 to point R_2 when nuclei move along either ''in'' or ''out'' parts of the classical trajectory, respectively. The first term relates to the case when the point R_1 is located in the ''in'' and the point R_2 is in the ''out'' part of the trajectory. It is important that for the retarded Green function the corresponding slowly varying amplitudes are the solutions of scattering equations in semiclassical form associated with normal $R(T)$-ordered motion of the nuclei along the classical trajectory in ''path'' potentials $U_{l_1}(R,\pm)$ and $U_{l_1}(R,+-)$ marked by index l_1. As in the case of the wave function the compiled index $l_1=\Omega_1,\ldots,\Omega_2$ performs all the states passed by the atoms during the fraction of the collision in intermediate state. The prime superscript in the sum sign shows that the summation is expanded over all intermediate states with fixed quantum numbers Ω_1 and Ω_2. The action integrals in Eq. (3.18) are defined as follows:

$$\mathcal{S}_{l_1}^{J_1}(R_2,R_1;+-)=\int_{R_{l_1}}^{R_2}k_{l_1}^{J_1}(R,+)dR+\int_{R_{l_1}}^{R_1}k_{l_1}^{J_1}(R,-)dR,$$

$$\mathcal{S}_{l_1}^{J_1}(R_2,R_1;-)=\int_{R_2}^{R_1}k_{l_1}^{J_1}(R,-)dR, \tag{3.19}$$

$$\mathcal{S}_{l_1}^{J_1}(R_2,R_1;+)=\int_{R_1}^{R_2}k_{l_1}^{J_1}(R,+)dR,$$

where the wave numbers dependent on R are defined as in Eqs. (3.17) with substitution of ''path'' potentials $U_{l_1}(R,\pm)$ or $U_{l_1}(R,+-)$. The ''path'' potentials are defined here as $U_{l_1}(R,\pm),U_{l_1}(R,+-)=U_{\Omega_1}(R),\ldots,U_{\Omega_2}(R)$, where the choice of adiabatic potential is determined by R location and by the type of classical trajectory ''out'' or ''in''. The slowly varying amplitudes $g_{l_1}^{J_1}(R_2,R_1;\pm)$ and $g_{l_1}^{J_1}(R_2,R_1;+-)$ can be found as the solution of scattering equations in semiclassical form, see Appendix A.

We substitute the semiclassical expansions (3.15),(3.18) in the expressions (3.14),(3.13) with the following assumptions. First, in the overlap integrals it is possible to keep only the terms that are slowly oscillating on R_1 and R_2 whose phases have a dependence on differences between action integrals relating to the lower and upper potentials. The rapidly oscillating terms, containing the sum of action integrals in exponential arguments, can be omitted in most of the practical situations. Indeed, for small frequency detunings (in comparison with recoil energy) it can be done because they oscillate much faster than slowly oscillating terms and make negligible contribution. In the opposite case for far off resonant detunings such terms relate to the situation when nuclear velocity changes the direction of motion after the photon absorption, a situation that is not compatible with a classical picture of optical transition. Therefore in the far wings of the spectral profile we neglect these terms because they cannot be satisfied under the conditions of stationary phase approximation, particularly, by the Franck-Condon principle. Secondly, we may simplify the angular momentum algebra by pointing out that for typical conditions the total angular momenta J,J_0,J_1 are much greater than unity and all of them have similar values. This makes it possible to use semiclassical asymptotic behavior of $6j$ symbols and Clebsch-Gordan coefficients and to expand the action integrals in Taylor's series as a function of total angular momentum. In Taylor's expansion we keep only the first derivative of the action integrals which are expressed by the classical angle of the rotation of the internuclear axis between bounding points. For example,

$$\frac{\partial}{\partial J_1}\mathcal{S}_{l_1}^{J_1}(R_2,R_1;+-)=-\xi_{l_1}^{J_1}(R_2,R_1;+-), \tag{3.20}$$

where $\xi_{l_1}^{J_1}(R_2,R_1;+-)$ is the rotation angle of the internu-

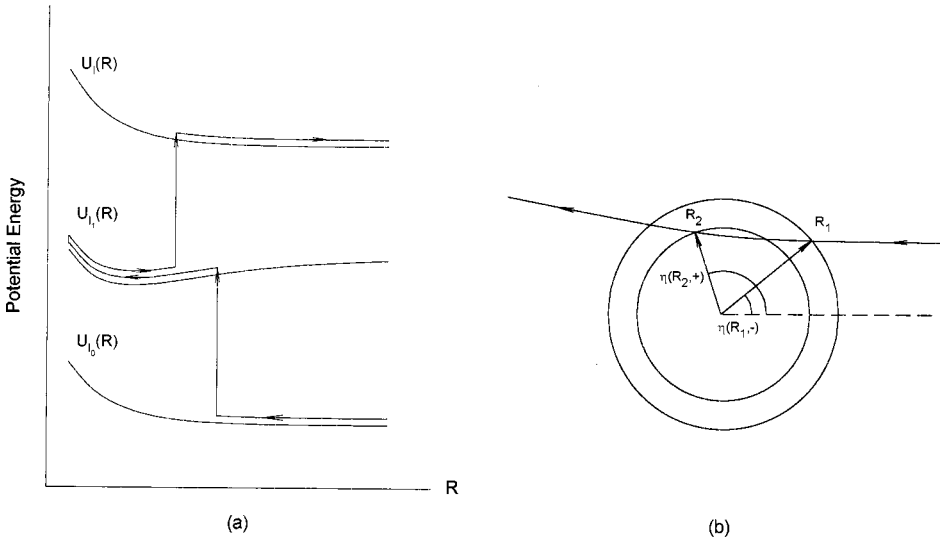

FIG. 1. (a) The schematic diagram showing the fractional optical collision with photon absorptions on ''in''-''out'' part of a classical trajectory. (b) The reference of deflection angles used in overlap integral (3.24).

clear axis from point R_1 to point R_2 located in ''in'' and ''out'' parts of the trajectory, respectively. We use similar notations for derivations of other action integrals. The relationship (3.20) lets us transform the sum over J,J_0,J_1,J_1' in Eq. (3.13) to the sum over only one angular momentum (impact parameter) and introduce in the theory such important characteristics of classical scattering as the deflection angles. It is important that all the deflection angles characterize the atomic motion in the ''path'' potential, i.e., they are compiled as the sum of different partial adiabatic contributions defined for each part of a real classical trajectory.

Finally the weighting factor $\tilde{Q}^{(X)}$ in Eq. (3.13) can be written as follows:

$$\tilde{Q}^{(X)}(\omega_1,\omega_2;\omega_1',\omega_2')=\frac{1}{2X+1}\sum_M\sum_{p_1p_1'}\sum_{p_2p_2'}(-)^{p_1+p_2'}\times C^{XM}_{1-p_1 1p_1'}C^{XM}_{1-p_2 1p_2'}\times\tilde{Q}_{p_1p_2;p_1'p_2'}(\omega_1,\omega_2;\omega_1',\omega_2'), \tag{3.21}$$

where the internal term is given by the sum of partial angular momentum contributions

$$\tilde{Q}_{p_1p_2;p_1'p_2'}(\omega_1,\omega_2;\omega_1',\omega_2')=\frac{\pi m^2}{\hbar^4k_0^2}\sum_J(2J+1)\times\frac{1}{2j_0+1}\sum_{\Omega_0\Omega}\langle\Omega|\mathcal{F}^J_{p_1p_2}(\omega_1,\omega_2)|\Omega_0\rangle\times\langle\Omega|\mathcal{F}^J_{p_1'p_2'}(\omega_1',\omega_2')|\Omega_0\rangle^*. \tag{3.22}$$

Here we introduced Dirac's notation for overlap integrals $\langle\Omega|\mathcal{F}^J_{p_1p_2}(\omega_1,\omega_2)|\Omega_0\rangle$. The motivation of such notation will be explained below, see Eq. (3.28).

The overlap integrals can be expanded in the sum of the following three terms:

$$\langle\Omega|\mathcal{F}^J_{p_1p_2}(\omega_1,\omega_2)|\Omega_0\rangle=\langle\Omega|\mathcal{F}^J_{p_1p_2}(\omega_1,\omega_2;+-)|\Omega_0\rangle+\langle\Omega|\mathcal{F}^J_{p_1p_2}(\omega_1,\omega_2;-)|\Omega_0\rangle+\langle\Omega|\mathcal{F}^J_{p_1p_2}(\omega_1,\omega_2;+)|\Omega_0\rangle. \tag{3.23}$$

Such an expansion has a clear physical nature. The first term, which is given by

$$\langle\Omega|\mathcal{F}^J_{p_1p_2}(\omega_1,\omega_2;+-)|\Omega_0\rangle=-\frac{im}{\hbar^2}e^{i\pi(J+1/2)}{\sum_{l_0}}'\sum_{l_1}\sum_{l}\int_{R^{(1)}}^{\infty}\int_{R^{(2)}}^{\infty}dR_1dR_2e^{i\Delta\mathcal{S}^J_{ll_1l_0}(R_2,R_1;+-)}\times\Big[(k^J_l(R_2,+)k^J_{l_1}(R_2,+)k^J_{l_1}(R_1,-)k^J_{l_0}(R_1,-)]^{-1/2}b^{J*}_l(R_2,+)(d^-_{\nu_2})_{\bar{\Omega}\Omega_2}g^J_{l_1}(R_2,R_1;+-)\times(d^-_{\nu_1})_{\Omega_1\bar{\Omega}_0}a^J_{l_0}(R_1,-)D^1_{\nu_2-p_2}\Big(-\frac{\pi}{2},-\eta^J_{l_1l_0}(R_2,+),\frac{\pi}{2}\Big)D^1_{\nu_1p_1}\Big(-\frac{\pi}{2},-\eta^J_{l_0}(R_1,-),\frac{\pi}{2}\Big), \tag{3.24}$$

describes the contribution coming from the attachment of the upper ''out'' and lower ''in'' running waves to the ''in-out'' part of the Green function. So, from a semiclassical point of view, it relates to the process when the first and the second photons

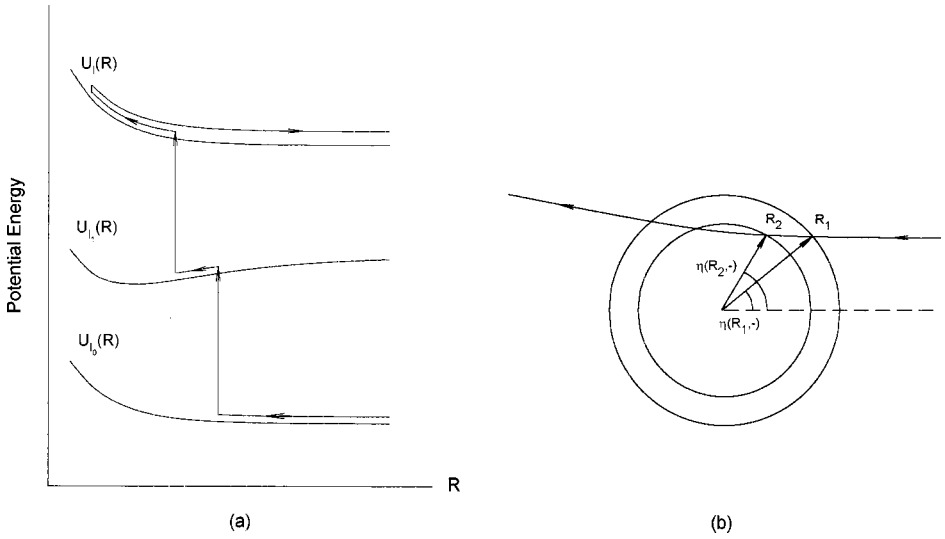

FIG. 2. (a) The schematic diagram showing the fractional optical collision with photon absorptions on ''in'' part of a classical trajectory. (b) The reference of deflection angles used in overlap integral (3.25).

are absorbed on ''in'' and ''out'' parts of the classical trajectory, respectively. This contribution as well as the reference of deflection angles $\eta^J_{l_1 l_0}(R_2,+)$ and $\eta^J_{l_0}(R_1,-)$ are shown in Fig. 1. The second term in Eq. (3.23), which is given by

$$\langle\Omega|\mathcal{F}^J_{p_1p_2}(\omega_1,\omega_2;-)|\Omega_0\rangle = -\frac{im}{\hbar^2}e^{i\pi(J+1/2)}\sum_{l_0}{}'\sum_{l_1}\sum_{l}{}'\int_{R^{(1)}}^{\infty}dR_1\int_{R^{(2)}}^{R_1}dR_2 e^{i\Delta\mathcal{S}^J_{ll_1l_0}(R_2,R_1;-)}$$
$$\times[k^J_l(R_2,-)k^J_{l_1}(R_2,-)k^J_{l_1}(R_1,-)k^J_{l_0}(R_1,-)]^{-1/2}{b_l}^{J*}(R_2,-)(d^{-}_{\nu_2})_{\bar{\Omega}\Omega_2}g^J_{l_1}(R_2,R_1;-)$$
$$\times(d^{-}_{\nu_1})_{\Omega_1\bar{\Omega}_0}a^J_{l_0}(R_1,-)D^1_{\nu_2-p_2}\left(-\frac{\pi}{2},-\eta^J_{l_1l_0}(R_2,-),\frac{\pi}{2}\right)D^1_{\nu_1p_1}\left(-\frac{\pi}{2},-\eta^J_{l_0}(R_1,-),\frac{\pi}{2}\right), \tag{3.25}$$

describes the contribution coming from the attachment of the upper ''in'' and lower ''in'' waves to the ''in'' part of the Green function. It assumes that both the photons are absorbed on the ''in'' part of the classical trajectory. This contribution as well as the reference of deflection angles $\eta^J_{l_1 l_0}(R_2,-)$ and $\eta^J_{l_0}(R_1,-)$ are shown in Fig. 2. The third term, which is given by

$$\langle\Omega|\mathcal{F}^J_{p_1p_2}(\omega_1,\omega_2;+)|\Omega_0\rangle = -\frac{im}{\hbar^2}e^{i\pi(J+1/2)}\sum_{l_0}{}'\sum_{l_1}\sum_{l}{}'\int_{R^{(1)}}^{\infty}dR_2\int_{R^{(2)}}^{R_2}dR_1 e^{i\Delta\mathcal{S}^J_{ll_1l_0}(R_2,R_1;+)}$$
$$\times[k^J_l(R_2,+)k^J_{l_1}(R_2,+)k^J_{l_1}(R_1,+)k^J_{l_0}(R_1,+)]^{-1/2}{b_l}^{J*}(R_2,+)(d^{-}_{\nu_2})_{\bar{\Omega}\Omega_2}g^J_{l_1}(R_2,R_1;+)$$
$$\times(d^{-}_{\nu_1})_{\Omega_1\bar{\Omega}_0}a^J_{l_0}(R_1,+)D^1_{\nu_2-p_2}\left(-\frac{\pi}{2},-\eta^J_{l_1l_0}(R_2,+),\frac{\pi}{2}\right)D^1_{\nu_1p_1}\left(-\frac{\pi}{2},-\eta^J_{l_0}(R_1,+),\frac{\pi}{2}\right), \tag{3.26}$$

describes the contribution coming from the attachment of the upper ''out'' and lower ''out'' waves to the ''out'' part of the Green function. It assumes that both the photons are absorbed on the ''out'' part of the classical trajectory. This contribution as well as the reference of deflection angles $\eta^J_{l_1 l_0}(R_2,+)$ and $\eta^J_{l_0}(R_1,+)$ are shown in Fig. 3. In the integrals (3.24)–(3.26) the lower limits $R^{(1)}$ and $R^{(2)}$ are the largest coordinates of the turning points taken for the paths l_1, l_0 and l, l_1, respectively.

The arguments of exponential functions in the overlap integrals (3.24)–(3.26) are defined as follows:

$$\Delta\mathcal{S}^J_{ll_1l_0}(R_2,R_1;+-) = \lim_{R,R_0\to\infty}\left\{\int_{R_2}^{R}k^J_l(R',+)dR' + \int_{R_{l_1}}^{R_2}k^J_{l_1}(R',+)dR' + \int_{R_{l_1}}^{R_1}k^J_{l_1}(R',-)dR' + \int_{R_1}^{R_0}k^J_{l_0}(R',-)dR' - kR - k_0R_0\right\},$$

$$\Delta\mathcal{S}^J_{l l_1 l_0}(R_2,R_1;-)=\lim_{R,R_0\to\infty}\left\{\int_{R_l}^{R}k_l^J(R',+)dR'+\int_{R_l}^{R_2}k_l^J(R',-)dR'+\int_{R_2}^{R_1}k_{l_1}^J(R',-)dR'+\int_{R_1}^{R_0}k_{l_0}^J(R',-)dR'-kR-k_0R_0\right\},\tag{3.27}$$

$$\Delta\mathcal{S}^J_{l l_1 l_0}(R_2,R_1;+)=\lim_{R,R_0\to\infty}\left\{\int_{R_2}^{R}k_l^J(R',+)dR'+\int_{R_1}^{R_2}k_{l_1}^J(R',+)dR'+\int_{R_{l_0}}^{R_1}k_{l_0}^J(R',+)dR'+\int_{R_{l_0}}^{R_0}k_{l_0}^J(R',-)dR'-kR-k_0R_0\right\}.$$

Taken with additional contribution $\pi(J+\frac{1}{2})$ these functions perform the finite increment of the total classical action evaluated in the ''path'' potential along the compiled path l_0,l_1,l, see Figs. 1–3.

It is useful to analyze the formal behavior of the overlap integrals (3.24)–(3.26) in the limit of small frequency detunings $\Delta_1=\omega_1-\omega_{10}$, $\Delta_2=\omega_2-\omega_{20}$, where ω_{10} and ω_{20} are the atomic resonant frequencies, in the conditions close to two-photon resonance $\Delta_1+\Delta_2=0$. For small detunings the total angular momenta J with large values give the main contribution in the total cross section. For large J and at the asymptote $R\to\infty$ we can estimate the overlap integrals in the straight trajectory approximation. In such a case the transformations of electronic wave functions caused by Coriolis nonadiabatic coupling are expressed in terms of pure rotation transformations from laboratory to molecular frame. The interatomic interaction is negligible and the projection of the electronic angular momentum on the z axis defined for initial or final helicity frame is conserved during the collision. Because the rotation transformation is unitary it is possible to express the overlap integrals in terms of matrix elements of the dipole moments in the atomic basis set with angular momentum eigenfunctions defined in the helicity frame

$$\langle\Omega|\mathcal{F}^J_{p_1p_2}(\omega_1,\omega_2)|\Omega_0\rangle\propto\sum_{\Omega_1}(-)^j\langle j-\Omega|d_{-p_2}|j_1\Omega_1\rangle\frac{1}{\Delta_1}\langle j_1\Omega_1|d_{p_1}|j_0\Omega_0\rangle.\tag{3.28}$$

The $\propto$ sign here means that the right side is proportional to the large overlap integral of the radial wave functions in the asymptotic domain and it approaches infinity at resonance. All the matrix elements in this expression are defined in the R-helicity frame with z-quantized axis along $-\mathbf{k}_0$. The asymptotic relationship (3.28) shows that the overlap integrals reduce to the usual transition amplitude of the two-photon absorption by free atom, which is estimated in the second order of perturbation theory. Dirac's notation emphasizes such asymptotic behavior of the overlap integrals.

Substituting the zero detuning asymptote of matrix elements (3.28) into Eqs. (3.22),(3.21), and then into Eq. (3.11), we can express the total cross section in the following form:

$$\tilde{\sigma}(\omega_1,\omega_2;\omega_1',\omega_2')\propto\sum_{X\Xi}(-)^{X+\Xi}\Phi_{X\Xi}(\mathbf{e}_1)\Phi_{X-\Xi}(\mathbf{e}_2)\times\frac{(-)^{j-j_0}}{(2j_0+1)}\begin{Bmatrix}1&1&X\\ j_1&j_1&j\end{Bmatrix}\times\begin{Bmatrix}1&1&X\\ j_1&j_1&j_0\end{Bmatrix}|d_{jj_1}|^2\frac{1}{\Delta_1\Delta_1'}|d_{j_1j_0}|^2,\tag{3.29}$$

which is in accordance with the general dependence of two-photon resonance photoabsorption on mutual laser polarization. Here d_{jj_1}, and $d_{j_1j_0}$ are the reduced matrix elements of the dipole moment and $\{\}$ denotes the $6j$ symbols, see [19].

However, we point out here that, in spite of realistic asymptotic behavior, the relationships (3.28) and (3.29) are

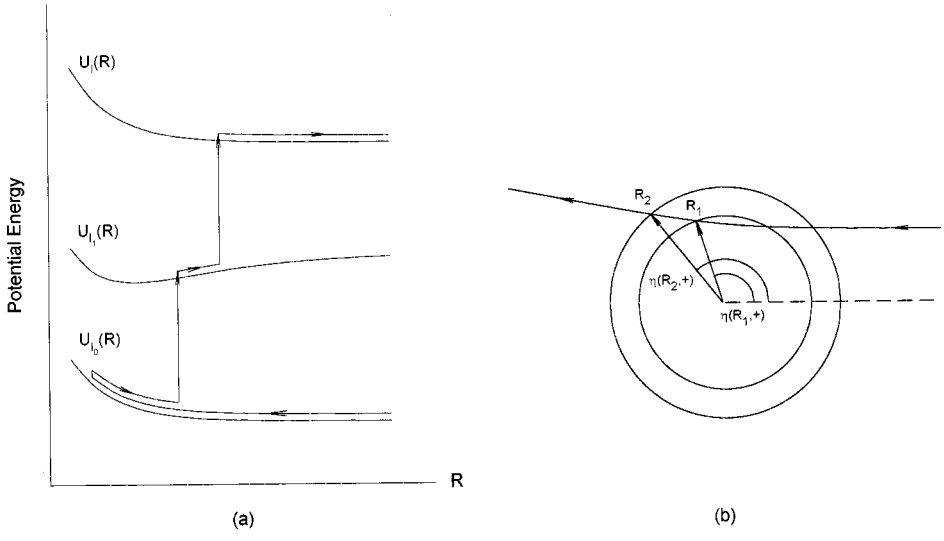

FIG. 3. (a) The schematic diagram showing the fractional optical collision with photon absorptions on ''out'' part of a classical trajectory. (b) The reference of deflection angles used in overlap integral (3.26).

not exactly compatible with the case of resonance photoabsorption. Such important effects as spontaneous decay of excited states and an interaction with other particles in long-term time scale were completely ignored in our analysis. Both the effects are responsible for the photoabsorption spectrum near the resonance, where it can be correctly described by Wigner-Weisskopf approximation. Actually, the relationship (3.28) shows only the right polarization dependence of the two-photon absorption in the resonance conditions but not the spectral profile itself. Therefore in the numerical calculations of the polarization-dependent spectrum based on Eqs. (3.21)–(3.26) we should restrict ourselves to the case when both the detunings Δ_1 and Δ_2 are comparable to or larger but not less than critical value $\tau_c^{-1} \sim \overline{v}/\rho_0$, where $\overline{v}$ is average recoil velocity. The critical time τ_c can be estimated in order of magnitude by the average time of collision.

C. Quasistatic picture of fractional optical collision

The qualitative and quantitative analysis of fractional optical collision can be simplified if the overlap integrals are evaluated in the stationary phase approximation. The typical conditions of the Franck-Condon approximation assume that all the detunings Δ_1, Δ_2, and $\Delta = \Delta_1 + \Delta_2$ are off resonant and much larger than τ_c^{-1}. We restrict our analysis to the situation when stationary points exist for both the transitions

$$U_{l_1}(R_1) - U_{l_0}(R_1) = \hbar\omega_1, \quad U_{l_1}(R_1') - U_{l_0}(R_1') = \hbar\omega_1', \qquad U_l(R_2) - U_{l_1}(R_2) = \hbar\omega_2, \quad U_l(R_2') - U_{l_1}(R_2') = \hbar\omega_2', \tag{3.30}$$

and we presume that the location of R_1, R_1' is separated (from the semiclassical point of view) from the location of R_2, R_2'. The definitions of Condon points shown by Eq. (3.30) allow the general form of the electric field correlation function and its spectrum, see Eqs. (2.6), (2.14), and (3.4). We emphasize here that for the light with general correlation properties the frequency ω_1 differs from ω_1' and ω_2 differs from ω_2', which leads to the difference in locations of Condon points R_1 and R_1' or R_2 and R_2'. However, we will neglect the distinction between them in the slowly varying preexponential factors. This can be substantiated by the fact that for our following analysis it is more interesting to consider the correlation function with narrow spectral profile near the average frequencies $\overline{\omega_1}$ and $\overline{\omega_2}$. As shown in [28] the correlation effects are most important if the difference $\omega_1 - \omega_1' = \omega_2' - \omega_2$ has the same order of magnitude as the scale $\Delta\tau^{-1}$, where $\Delta\tau$ is the time of the classical motion between the Condon points. In such a case and in the semiclassical conditions of an atomic motion the distinction in locations of R_1 and R_1' or R_2 and R_2' is negligible for preexponential factors. However, it can be very important in the arguments of exponential functions containing the large action integrals.

For large frequency detunings all the Condon points are located inside the so-called decoupling sphere, i.e., in Hund's *a* region, see Appendix A. For simplicity we will restrict ourselves to the practically important situation when the slow variations on R amplitudes of the Green function (3.18) are determined by simple adiabatic dynamics and given by

$$g_{l_1}^J(R_2,R_1;-) = g_{\Omega_2\Omega_1}^J(R_2,R_1;-) = \delta_{\Omega_2\Omega_1}, \quad R_2 < R_1$$

$$g_{l_1}^J(R_2,R_1;+) = g_{\Omega_2\Omega_1}^J(R_2,R_1;+) = \delta_{\Omega_2\Omega_1}, \quad R_2 > R_1 \tag{3.31}$$

$$g_{l_1}^J(R_2,R_1;+-) = g_{\Omega_2\Omega_1}^J(R_2,R_1;+-) = \delta_{\Omega_2\Omega_1}.$$

Such an assumption is not critical for our approach, but it makes the following discussion more clear. Moreover, in the quasistatic conditions of the photoexcitation, we can neglect in the product of the overlap integrals those interference terms which disappear after the averaging over impact parameter (angular momentum) because of quasiclassical oscillations. Also the nonadiabatic dynamics of lower and upper states of the fractional collision becomes unimportant. Indeed, any nonadiabatic transformation describing the evolution of the electronic subsystem in the molecular regions is an example of a unitary transformation, so the square of transition amplitude $|a_{l_0}(R_1;\pm)|^2$ or $|b_l(R_1;\pm)|^2$ reduces to unity because of the averaging over initial and final electronic states.

Consider the spectral profile of the cross section written in the form (3.11). Evaluating the semiclassical overlap integrals in the stationary phase approximation, the partial cross section $\tilde{Q}^{(X)}$, which describes both the polarization and spectral dependencies of the fractional collision, can be expressed as follows:

$$\begin{aligned}\tilde{Q}^{(X)}(\omega_1,\omega_2;\omega_1',\omega_2') = \sum_l 2\pi \int_0^{\rho_l} \rho d\rho \tilde{w}_l^{(1)}(\rho)\tilde{w}_l^{(2)}(\rho) \frac{1}{(2j_0+1)(2X+1)} \sum_{\overline{\Xi}} \sum_{\overline{\nu}_1\overline{\nu}_1'} \sum_{\overline{\nu}_2\overline{\nu}_2'} (-)^{\overline{\nu}_2'+\overline{\nu}_1} \\ \times C^{X\overline{\Xi}}_{1\overline{\nu}_2 1-\overline{\nu}_2} C^{X\overline{\Xi}}_{1-\overline{\nu}_1 1\overline{\nu}_1'} [\exp\{iS_l^\rho(\omega_1,\omega_2;+-) - iS_l^\rho(\omega_1',\omega_2';+-)\} d^X_{\overline{\Xi}\overline{\Xi}}(\xi_l^\rho(R_2,R_1;+-)) \\ + \exp\{iS_l^\rho(\omega_1,\omega_2;-) - iS_l^\rho(\omega_1',\omega_2';-)\}\theta(R_1-R_2) d^X_{\overline{\Xi}\overline{\Xi}}(\xi_l^\rho(R_2,R_1;-)) \\ + \exp\{iS_l^\rho(\omega_1,\omega_2;+) - iS_l^\rho(\omega_1',\omega_2';+)\}\theta(R_2-R_1) d^X_{\overline{\Xi}\overline{\Xi}}(\xi_l^\rho(R_2,R_1;+))].\end{aligned} \tag{3.32}$$

The outer sum in this expression is expanded over all possible classical paths l crossing the Condon points R_1 and R_2 as well as over all the combinations of the Condon points if there is more than one for each detuning. To simplify notation we denote by l here and below the set ll_1l_0. The cross section (3.32) is written as the integral over impact parameter $\rho=(J+1/2)/k_0$ instead of a sum over total angular momentum J, as seems more reasonable in a classical description of atomic collisions. We note here that because of angular momentum conservation the definition of impact parameter differs for the lower, intermediate, and upper states. The integral is bounded by the maximum value ρ_l for the limit trajectory touching the inner Condon points R_1 or R_2. Wigner d functions are defined as in Ref. [19] and they depend on the deflection angles referred to the classical trajectories between the Condon points. In the arguments of the nonexponential functions in integral (3.32) we assume the average location of the Condon points and neglect the difference between R_1 and R_1' or R_2 and R_2'. However, we distinguish the difference in the arguments of the exponential functions because of the large value of the action integrals.

The dependence of the action integrals on the light frequencies comes from two effects: from the variation in the location of Condon points and from the dependence of the action on recoil energy. Showing all the arguments in the classical action we can express the frequency dependence as follows:

$$S_l^{\rho}(\omega_1,\omega_2;\pm)=\Delta S^{\rho}_{ll_1l_0}(R_2(\omega_2),R_1(\omega_1);E_0+\hbar\omega_1;\pm),$$
$$S_l^{\rho}(\omega_1,\omega_2;+-)=\Delta S^{\rho}_{ll_1l_0}(R_2(\omega_2),R_1(\omega_1);E_0+\hbar\omega_1;+-), \tag{3.33}$$

where E_0 is the initial recoil energy and the action integrals in the right side are defined by Eqs. (3.27). In the case of stationary photoexcitation the spectrum of the correlation function is restricted by the condition $\omega_1+\omega_2=\omega_1'+\omega_2'$. Thus in spite of the fact that each of the action integrals contributed in Eq. (3.32) depends on both the frequencies, the difference between the actions actually depends only on one frequency detuning, $\omega_1-\omega_1'=\omega_2'-\omega_2$.

The probabilities of photoexcitation at each Condon point are given by

$$\tilde{w}_l^{(1)}(\rho)=\frac{1}{\hbar^2}[(d_{\bar{\nu}_1})_{\Omega_1\bar{\Omega}_0}\tau_l^{(1)}(\rho)]^2,$$
$$\tilde{w}_l^{(2)}(\rho)=\frac{1}{\hbar^2}[(d_{\bar{\nu}_2})_{\bar{\Omega}\Omega_2}\tau_l^{(2)}(\rho)]^2, \tag{3.34}$$

where the tilde indicates that these parameters become real probabilities only after multiplying the dipole moment matrix elements $(d_{\bar{\nu}_1})_{\Omega_1\bar{\Omega}_0}$ and $(d_{\bar{\nu}_2})_{\bar{\Omega}\Omega_2}$ on the electric field amplitudes. The transition times of the vicinities of the Condon points are defined as follows:

$$\tau_l^{(i)}(\rho)=\left(\frac{2\pi\hbar}{\Delta F^{(i)}v_l^{(i)}(\rho)}\right)^{1/2}, \tag{3.35}$$

with $i=1,2$. Here $\Delta F^{(1)}$, $\Delta F^{(2)}$ are the differences between the slopes of upper and lower potentials at the Condon points R_1, R_2 and $v_l^{(1)}(\rho)$, $v_l^{(2)}(\rho)$ are the radial velocities at these points,

$$v_l^{(i)}(\rho)=\left[\frac{2E}{m}\left(1-\frac{U_l(R_i)}{E}-\frac{\rho^2}{R_i^2}\right)\right]^{1/2}. \tag{3.36}$$

We assume that there is no difference for all the parameters defined by Eqs. (3.34)–(3.36) with the similar parameters marked by primes.

The vector indices $\bar{\nu}_1,\bar{\nu}_1'$ and $\bar{\nu}_2,\bar{\nu}_2'$ of the dipole moments in Eq. (3.32) relate to the molecular frame and as follows from Eq. (3.31) we have the following selection rule: $\bar{\nu}_1=-\bar{\nu}_2$ and $\bar{\nu}_1'=-\bar{\nu}_2'$, permitting $\bar{\nu}_1=\bar{\nu}_1'$ and $\bar{\nu}_2=\bar{\nu}_2'$ as well as the interference contribution $\bar{\nu}_1=-\bar{\nu}_1'$, and $\bar{\nu}_2=-\bar{\nu}_2'$, if the excitation is initiated through the $^1\Sigma_0\rightarrow{}^1\Pi_1\rightarrow{}^1\Sigma_0$ channel. Such an interference contribution does not disappear after the averaging over impact parameter. The inner sum in the expression (3.32) over the vector indices is noninvariant and it should be evaluated in the molecular frame. The result depends strongly on the symmetry of the excited transitions and the polarization-dependent part of the cross section can change even the sign for different types of Franck-Condon transitions. The presence of d functions in Eq. (3.32) can be interpreted as the rotational transformation of the irreducible components of the light density matrix (either for the first or for the second photons) along the classical trajectory following adiabatic change in orientation of the molecular frame. So, if we treat the fractional optical collision in the recoil limit approximation with less influence of rotation effects, we obtain from Eq. (3.32) the simple qualitative estimation of the polarization dependence of the process. We will illustrate this by practical calculations presented in the next section.

The spectral dependence of the cross section is presented in Eq. (3.32) by two different effects. First, the spectral dependence appears from the frequency dependence of the Condon point locations. Secondly, and less obviously, this can appear also because of the correlation between the first and the second photoabsorption events. This can be seen when we approximate the difference in action integrals by the first increment of the action with respect to its energy argument. We obtain that the corresponding action derivative is just the classical propagation time of the atomic nuclei between the points R_1 and R_2. Then we see that the correlation spectral dependence can take place if the system is probed by the light sources correlated on the time scale comparable with the natural time delay between photoabsorption events. We plan to discuss the problem of the correlation control of fractional optical collision in more detail in future [28].

IV. APPLICATION TO Mg-He ($3S^2\,{}^1S_0\rightarrow 3P\,{}^1P_1\rightarrow 5S\,{}^1S_0$, $4D\,{}^1D_2$) FRACTIONAL OPTICAL COLLISION

In contrast to the single-photon transition, which can often be well understood in a quasistatic model, the two-photon excitation is more complicated and less obvious for numerical calculations. Even in quasistatic conditions it is common for the stationary phase point to exist only for one

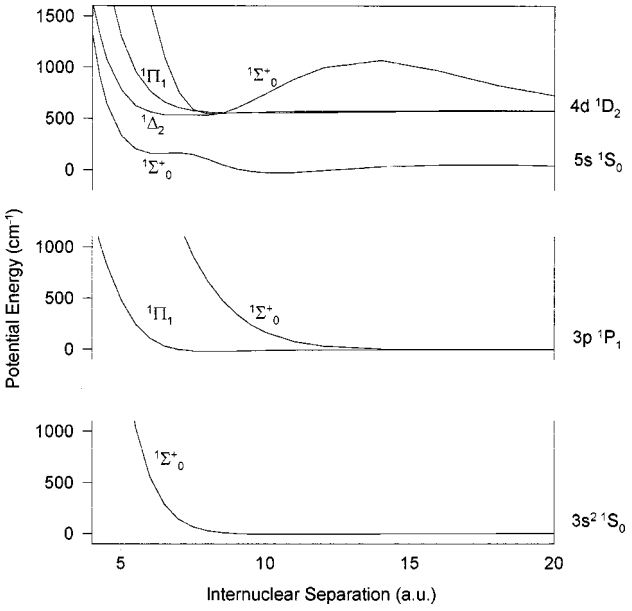

FIG. 4. The Mg-He singlet potentials from [29].

optical transition. It is also possible that a stationary phase point exists for two-photon transitions and it does not exist or makes negligible contribution for any single-photon transitions. So the population of upper molecular state can take place without population of intermediate molecular states. There are also many situations with interference and competition between single- and two-photon Condon transitions.

Our choice of Mg-He fractional optical collision for numerical calculations is motivated by the following reasons. First of all, the interatomic interaction of helium with near Rydberg states of magnesium can be calculated with better accuracy than for other heavy rare-gas partners. Second, the quasimolecule Mg-He is characterized by shallow potential wells for excimer states, which makes it possible to ignore the resonance scattering caused by shape resonances and to approximate molecular electronic wave functions by atomic ones in a broader range of internuclear separations. Third, because of small reduced mass for the Mg-He pair the role of interference effects as well as the precision of quasistatic approximation can be tested here in a most critical situation.

The most difficult point of numerical calculations is the evaluation of rapidly oscillating overlap integrals (3.24)–(3.26). To define action integrals and deflection angles we used Mg-He interaction potentials calculated by Czuchaj [29], which are shown in Fig. 4. We assumed optical excitation by coherent noncorrelated laser pulses, which is a common experimental situation, see [13]. In such a case the light correlation function of the second order (2.6) can be expressed as a product of the first order correlation functions, and the spectral profile (3.11) as well as the transition overlap integrals, considered as a function of the frequencies, should be taken at coincidence frequencies $\omega_1=\omega_1'$ and $\omega_2=\omega_2'$. In numerical procedure we improve the convergence of the overlap integrals near the classical turning points by substituting the semiclassical representation of the wave functions by Airy function in accordance with general recommendation in quantum mechanics [30]. Such a correction is negligible if we evaluate the overlap integrals in the conditions close to the stationary phase case, when the regions with slowly oscillating integrands determine mainly the magnitude of the integrals. However, it can be rather important if we evaluate the integrals for the long-range trajectories with large angular momentum (impact parameter), where there is no stationary phase region, to reproduce the orthogonality of the wave functions with better accuracy.

The calculations have been made for optical collisions with excitation of magnesium atoms from the $3s^2\,^1S_0$ lower state up to $5s\,^1S_0$ and $4d\,^1D_2$ upper states via the $3p\,^1P_1$ intermediate state. The corresponding semiclassical expansions of the retarded Green function, correlated with the $3p\,^1P_1$ state, is given in Appendix A. The semiclassical representation of the radial wave functions, correlated with the $4d\,^1D_2$ state, is shown in Appendix B. Let $\sigma_\parallel^J(\Delta_1,\Delta_2)$ and $\sigma_\perp^J(\Delta_1,\Delta_2)$ be the partial cross sections, considered as functions of the frequency detunings, for $\mathbf{e}_1\|\mathbf{e}_2$ and for $\mathbf{e}_1\perp\mathbf{e}_2$, respectively. Their representations by the transition overlap integrals can be easily derived from the general expressions of Sec. III B. From the experimental point of view, in a cell experiment the polarization ratio can be defined for the total cross section only and it is given by

$$P_L=P_L(\Delta_1,\Delta_2)=\frac{\sigma_\parallel(\Delta_1,\Delta_2)-\sigma_\perp(\Delta_1,\Delta_2)}{\sigma_\parallel(\Delta_1,\Delta_2)+\sigma_\perp(\Delta_1,\Delta_2)}, \quad (4.1)$$

where

$$\sigma_\parallel(\Delta_1,\Delta_2)=\sum_J \sigma_\parallel^J(\Delta_1,\Delta_2),$$
$$\sigma_\perp(\Delta_1,\Delta_2)=\sum_J \sigma_\perp^J(\Delta_1,\Delta_2) \quad (4.2)$$

are the total cross sections. However, from a theoretical point of view, it is very useful to discuss also the angular momentum behavior of the polarization ratio, because for certain values of the total angular momentum J the numerical results can be better understood. So for the simplest optical excitation channel up to $5s\,^1S_0$ we have made a partial wave analysis to discuss the angular momentum dependence of the cross sections and the polarization ratio as well.

The plot in Fig. 5(a) shows the angular momentum dependence of the partial cross sections $\sigma_\parallel^J(\Delta_1,\Delta_2)$ and $\sigma_\perp^J(\Delta_1,\Delta_2)$ calculated at the recoil energy 450 K for the detunings $\Delta_1=30\,\mathrm{cm}^{-1}$ and $\Delta_2=-100\,\mathrm{cm}^{-1}$. There is the well isolated stationary phase point relating to the transition $3p\,^1\Sigma_0^+\rightarrow 5s\,^1\Sigma_0^+$, which is $R_2\sim 11$ a.u. In spite of the fact that in the first photoexcitation step on the transition $3s^2\,^1\Sigma_0^+\rightarrow 3p\,^1\Sigma_0^+$ there is also the stationary phase point located at $R_1\sim 12$ a.u., its vicinity does not really determine the full magnitude of the overlap integrals because for such small detuning the transition probability has the same order in the entire asymptotic region $R\rightarrow\infty$. Because the second transition can be made on either ''in'' or ''out'' parts of the classical trajectory, there is a strong interference contribution between two possible paths. The dependence of the cross sections on J shows the oscillating behavior caused by the interference and it has the strongest maximum at $J\simeq 40$. This maximum relates to the special trajectory where there is a coincidence of the Condon point with the turning point. The

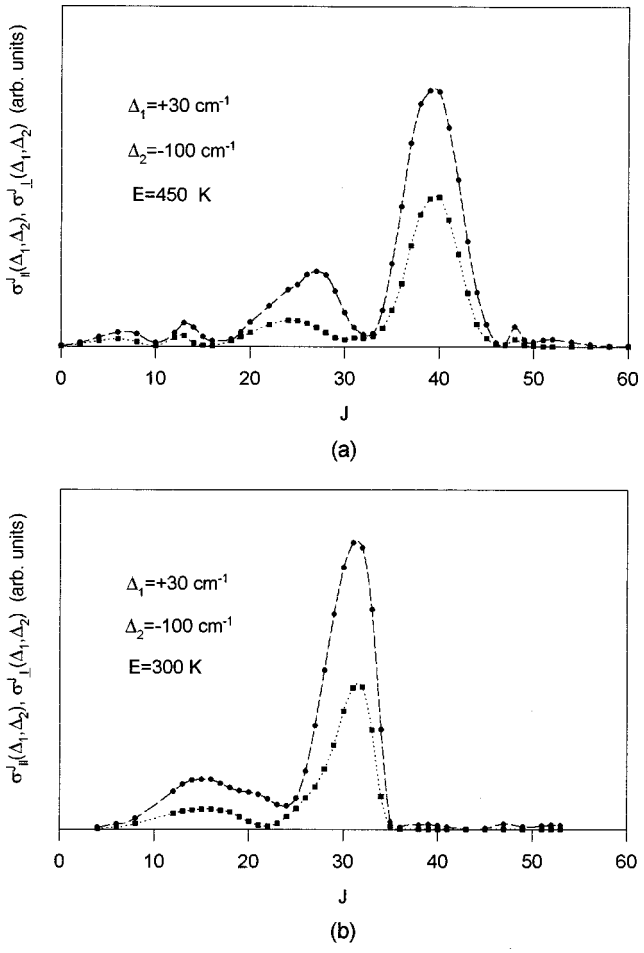

FIG. 5. Partial cross sections $\sigma^J_{\|}(\Delta_1,\Delta_2)$ (dashed line) and $\sigma^J_{\perp}(\Delta_1,\Delta_2)$ (dotted line) for Mg-He fractional optical collision $3s^2\,{}^1S_0 \rightarrow 3p\,{}^1P_1 \rightarrow 5s\,{}^1S_0$ for detunings $\Delta_1 = +30\,\mathrm{cm}^{-1}$, $\Delta_2 = -100\,\mathrm{cm}^{-1}$, and for recoil energies $E = 450\,\mathrm{K}$ (a) and $E = 300\,\mathrm{K}$ (b).

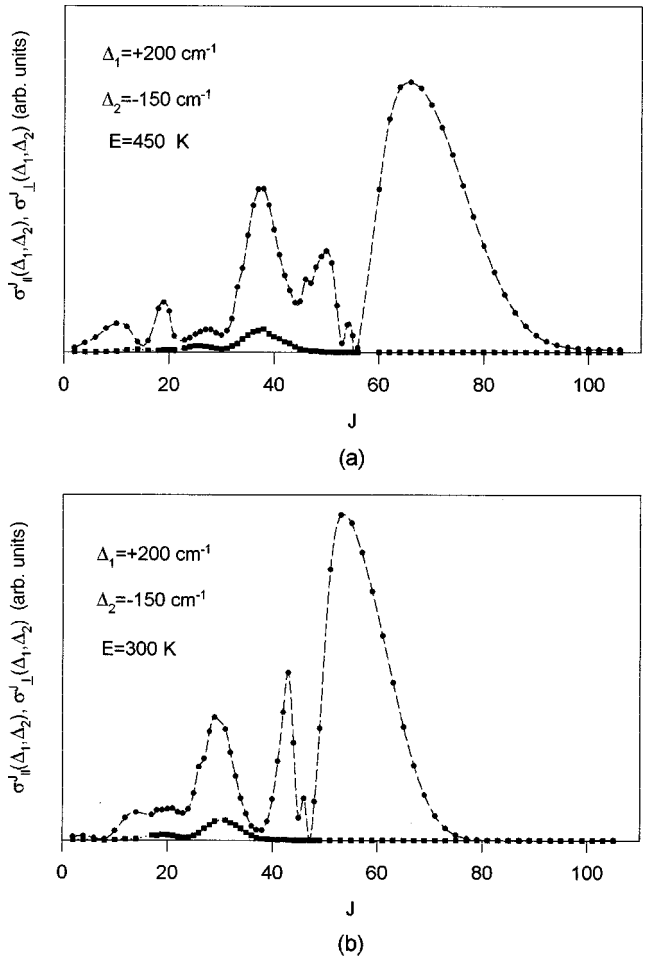

FIG. 6. Same as in Fig. 5 for detunings $\Delta_1 = +200\,\mathrm{cm}^{-1}$, $\Delta_2 = -150\,\mathrm{cm}^{-1}$.

quasistatic approximation averaging the interference oscillation can fit here for the inner angular momenta less than 40. The polarization ratio in such an approximation can be estimated using the expressions of Sec. III C, if we associate R_1 with decoupling sphere R_d. For a recoil limit it gives the polarization ratio close to $\frac{1}{2}$ which is in accordance with the polarization ratio obtained in full numerical calculations, 0.35. The interesting peculiarity in the dependence of the partial cross sections as a function of the angular momentum is that even for large $J > 40$ there is a sequence of small but attenuating maxima in the dependence of $\sigma^J_{\|}(\Delta_1,\Delta_2)$ on J caused by long-range exchange interaction in the $5s\,{}^1\Sigma_0^+$ state. In Fig. 5(b) we show the comparative dependences of $\sigma^J_{\|}(\Delta_1,\Delta_2)$ and $\sigma^J_{\perp}(\Delta_1,\Delta_2)$ on J for the same detunings as in Fig. 5(a) but for the recoil energy $E = 300\,\mathrm{K}$. All the physical peculiarities in the behavior of the cross sections here are similar to the case of Fig. 5(a) with slight differences in the locations of the maxima. The differences are caused mainly by the dependence of the locations of the turning points on the recoil energy. The polarization ratio in this case is 0.41, which is even closer to the recoil limit estimation than for the energy $E = 450\,\mathrm{K}$.

The plots in Fig. 6 show the more complicated situation. For the dependencies shown here the significant contribution in the overlap integrals comes from the area R_1, $R_2 \sim R_0$, where R_0 is the solution of $\hbar\omega_1 + \hbar\omega_2 = U(R_0) - U_0(R_0)$, where $U_0(R)$ and $U(R)$ are the potentials for $3s^2\,{}^1\Sigma_0^+$ and for $5s\,{}^1\Sigma_0^+$ states, respectively. Due to long-range repulsive interactions, caused by exchange forces, for Σ terms correlated with $5s$ and $4d$ electronic shells, see Fig. 4, there is a possibility to absorb the photons in a two-photon Condon transition if the sum of the detunings Δ_1 and Δ_2 is positive. In addition to the two-photon Condon transition it is also possible to absorb the photons in successive single-photon Condon transitions. The plots in Fig. 6 demonstrate the interference and the comparative contribution coming from two-step single-photon and one-step two-photon excitation channels. We consider the example when single-photon transitions take place via the $3p\,{}^1\Sigma_0^+$ intermediate state. The dependencies shown in Fig. 6 are plotted for the detunings $\Delta_1 = 200\,\mathrm{cm}^{-1}$ and $\Delta_2 = -150\,\mathrm{cm}^{-1}$ and for the recoil energies 450 K [in Fig. 6(a)] and 300 K [in Fig. 6(b)]. There are three stationary phase points: two single-photon Condon points located at 9.7 and 10.5 a.u. for the transitions $3s^2\,{}^1\Sigma_0^+ \rightarrow 3p\,{}^1\Sigma_0^+$ and $3p\,{}^1\Sigma_0^+ \rightarrow 5s\,{}^1\Sigma_0^+$, respectively, and one two-photon Condon point located at 18 a.u. for the transition $3s^2\,{}^1\Sigma_0^+ \rightarrow 5s\,{}^1\Sigma_0^+$. We chose the detuning in such a way that the two-photon Condon point would be located near the maximum of the barrier in the $5s\,{}^1\Sigma_0^+$ poten-

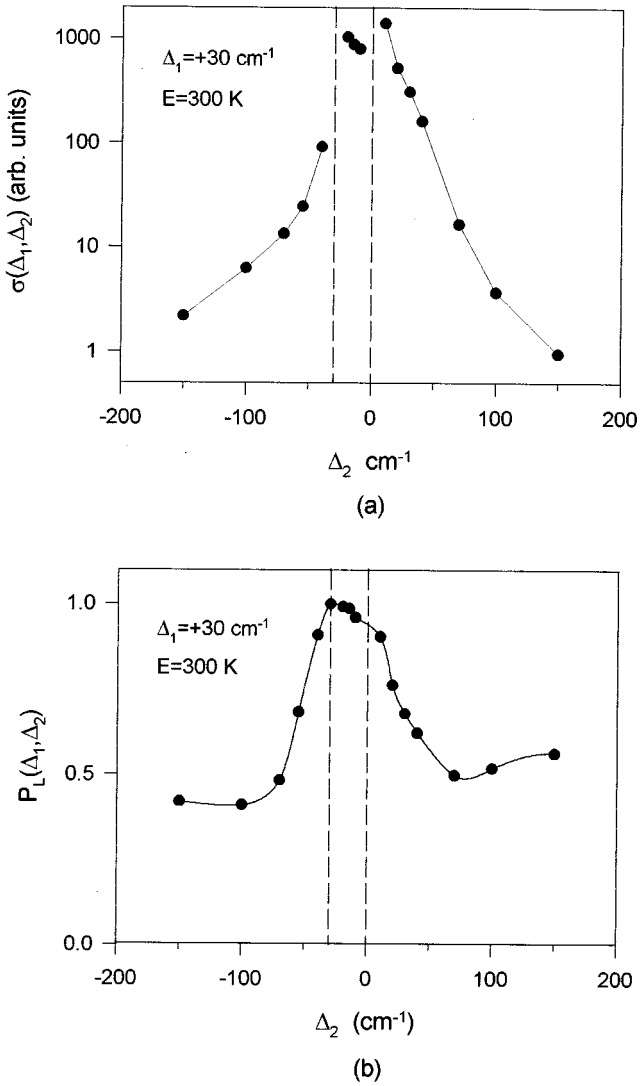

FIG. 7. The spectra of the total cross section (a) and of the polarization ratio (b) as a function of detuning Δ_2 for Mg-He $3s^2\,{}^1S_0 \rightarrow 3p\,{}^1P_1 \rightarrow 5s\,{}^1S_0$ fractional optical collision for detuning $\Delta_1 = +30\ \mathrm{cm}^{-1}$ and for recoil energy $E = 300$ K.

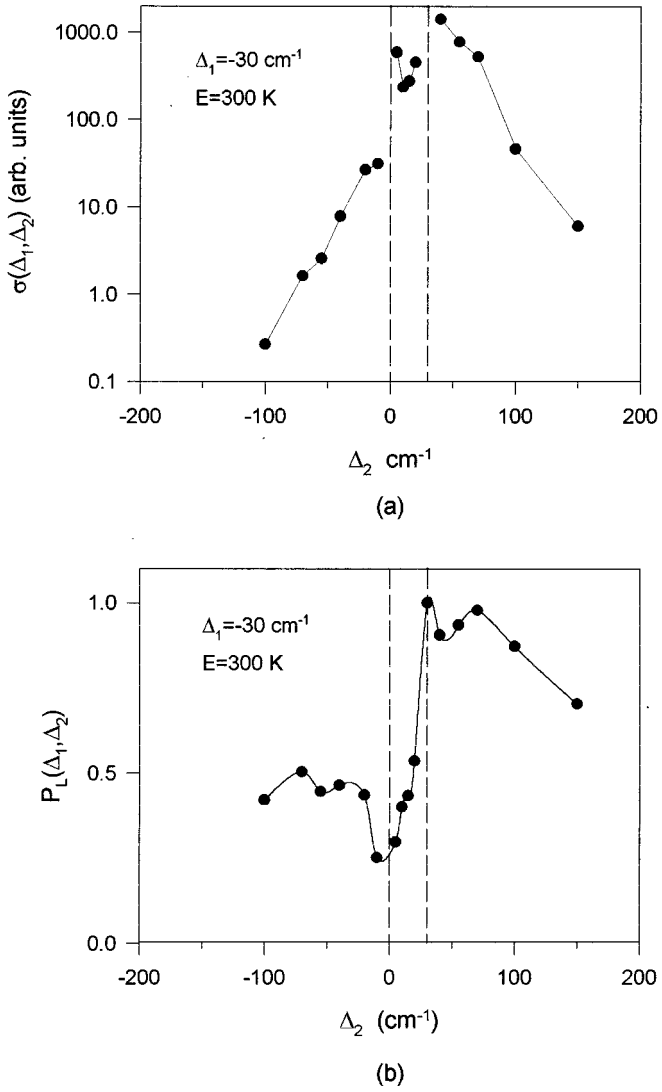

FIG. 8. Same as in Fig. 7 for detuning $\Delta_1 = -30\ \mathrm{cm}^{-1}$.

tial. As we see from the dependencies shown in Fig. 6 there is a broad maximum for the partial cross sections $\sigma_{\parallel}^{J}(\Delta_1,\Delta_2)$ and $\sigma_{\perp}^{J}(\Delta_1,\Delta_2)$ near the angular momenta $J \sim 60$–70 [Fig. 6(a)] and near 50–60 [Fig. 6(b)], which are determined by the two-photon Condon transitions for the long-range trajectories with large impact parameter. The oscillating behavior of the partial cross sections for smaller angular momenta indicate the interference effects as well as the contribution of single-photon Condon transitions. The important peculiarity of the two-photon Condon transition is that the partial polarization ratio rises to unity here. That is clear because in such a case the sum over all the intermediate Zeeman electronic states reduces to its invariant form like it does in two-photon photoabsorption by a free atom, and the polarization dependence turns out to be the same as for the free atom also.

In Figs. 7 and 8 we show the spectral dependencies of the polarization-independent total cross section

$$\sigma(\Delta_1,\Delta_2) = \sigma_{\parallel}(\Delta_1,\Delta_2) + 2\sigma_{\perp}(\Delta_1,\Delta_2) \qquad (4.3)$$

as well as the polarization ratio for the fractional optical collision $3s^2\,{}^1S_0 \rightarrow 3p\,{}^1P_1 \rightarrow 5s\,{}^1S_0$ calculated at recoil energy 300 K. The calculated spectra are presented for two detunings $\Delta_1 = +30\ \mathrm{cm}^{-1}$ (Fig. 7) and $\Delta_1 = -30\ \mathrm{cm}^{-1}$ (Fig. 8) as a function of the second detuning Δ_2. As follows from the numerical results the polarization ratio is positive and has a large order in all the spectral domains. Near the two-photon resonances $\Delta_1 + \Delta_2 \rightarrow 0$ it rises to unity.

The experimental data exist for Mg-Ne, Ar fractional optical collisions [13]. If we presume that the behavior of the potentials for the Mg-Ne pair is approximately like that for the Mg-He pair, we can obtain that our calculated spectra show behavior similar to Mg-Ne experimental results. For example, for negative detuning $\Delta_1 = -30\ \mathrm{cm}^{-1}$ we obtain nonmonotonic dependence of the polarization ratio in the wings of Δ_2, which is similar to P_L experimental spectra for Mg-Ne. As follows from the dependence plotted in Fig. 8(b) there is a two-photon Franck-Condon transition for $\Delta_2 > 0$ which manifests itself when P_L approaches unity. For negative Δ_2 there is some rise of the polarization ratio in a spectral domain of the red wing near the zero detuning. Such behavior of the polarization is in accordance with experimental results [13]. It is most interesting here that the polar-

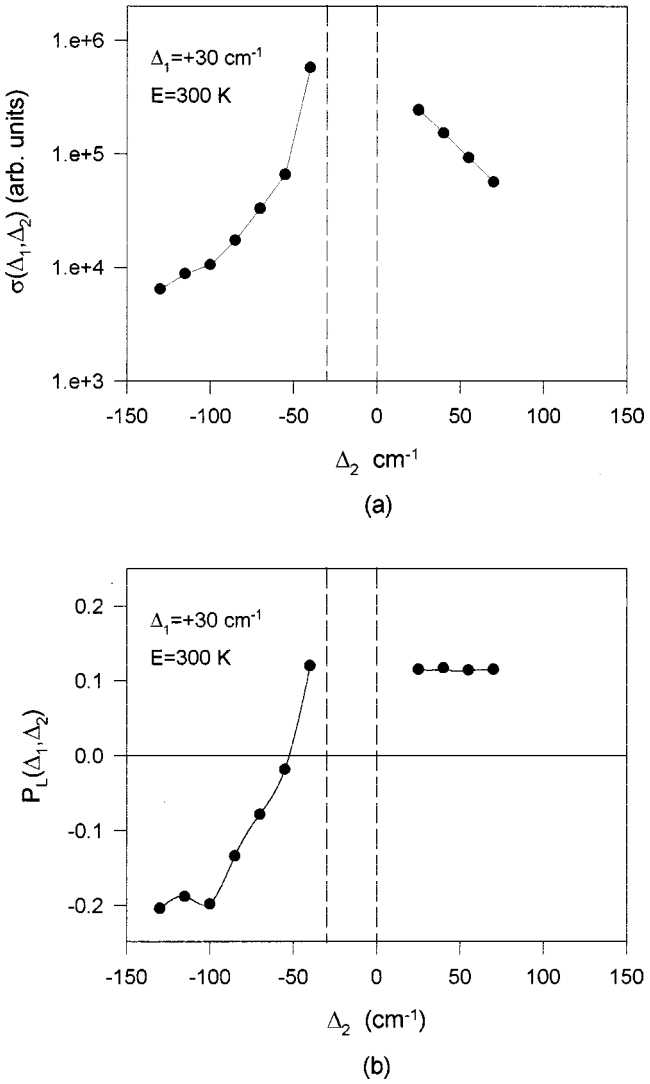

FIG. 9. The spectra of the total cross section (a) and of the polarization ratio (b) as a function of detuning Δ_2 for Mg-He $3s^2\,{}^1S_0 \rightarrow 3p\,{}^1P_1 \rightarrow 4d\,{}^1D_2$ fractional optical collision for detuning $\Delta_1 = +30\,\mathrm{cm}^{-1}$ and for recoil energy $E = 300$ K.

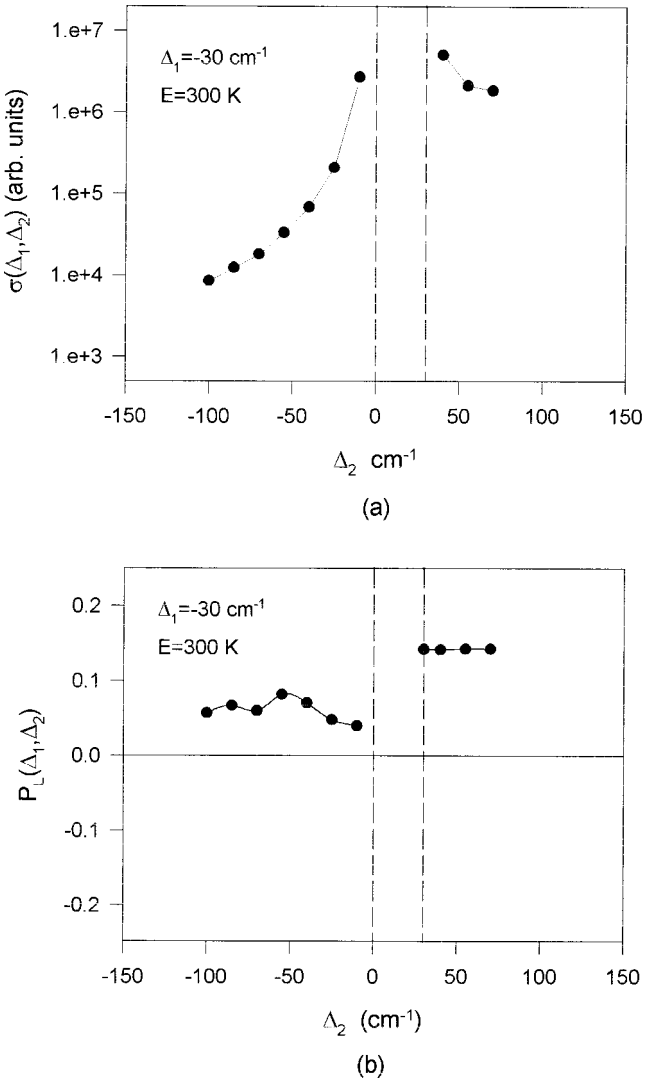

FIG. 10. Same as in Fig. 9 for detuning $\Delta_1 = -30\,\mathrm{cm}^{-1}$.

ization with photon absorption in a wing is greater than at $\Delta_2 = 0$, i.e., in direct resonance absorption of polarized atoms. Again such peculiarity in spectral behavior can be explained by the presence of some contribution coming from the two-photon Franck-Condon transition which is not sensitive to rotation depolarization.

The case of $3s^2\,{}^1S_0 \rightarrow 3p\,{}^1P_1 \rightarrow 4d\,{}^1D_2$ fractional collision is more complicated because of more channels involved in the process. The important peculiarity here is that, due to long-range exchange interactions in the $4d\,{}^1\Sigma_0^+$ state, we should consider two decoupling spheres restricting the influence of the Coriolis forces. The corresponding semiclassical expansion of the radial wave functions correlated with $4d\,{}^1D_2$ is given in Appendix B. Because the partial wave analysis is less obvious here, in Figs. 9 and 10 we present only the spectral dependencies of the total cross sections $\sigma(\Delta_1,\Delta_2)$, given by Eq. (4.3), and of the polarization ratio for the same detunings as in Figs. 7 and 8. A common feature in the behavior of the total cross section as a function of frequency detuning, which is shown in Figs. 9(a) and 10(a), is in an asymmetry of its spectral profile. The cross section is typically bigger in the blue wing of the full detuning $\Delta_1 + \Delta_2$ because the main contribution comes here from direct excitation via two-photon Franck-Condon transition to the $4d\,{}^1\Sigma_0^+$ state.

The spectral dependence of the polarization ratios is shown in Figs. 9(b) and 10(b). For the two-photon resonance $\Delta_1 + \Delta_2 \rightarrow 0$ the polarization ratio approaches $\frac{1}{7}$, which is in accordance with the polarization dependence of the two-photon absorption by unperturbed atoms. By tuning in the wings we partly break the atomic symmetry and select positive or negative contributions coming to $\frac{1}{7}$. This is illustrated by the behavior of the polarization ratio shown in Figs. 9(b) and 10(b). In the blue wing the polarization ratio is almost constant, which is due to the dominant role of direct two-photon Condon transitions to the $4d\,{}^1\Sigma_0^+$ state, leading to the same value of the polarization ratio as in the resonance case, i.e., $\frac{1}{7}$. At the same time, for the blue wing the successive single-photon Condon transitions to the $4d\,{}^1\Sigma_0^+$ via $3p\,{}^1\Pi_1$, ${}^1\Sigma_0^+$ states are also possible and they can give a larger positive polarization ratio. However, in the case of rather small first detuning $\Delta_1 = \pm 30\,\mathrm{cm}^{-1}$ and for a light foreign atom such as He the role of these transitions is not so important as

for heavier atoms where they lead to a slight but clear rise of the polarization ratio in the blue wing of the spectrum, see [8].

In contrast to the blue wing, in the red wing the polarization ratio decreases and becomes even negative for partial cross sections relating to small impact parameters. That indicates that the main contribution comes here from successive photoexcitations up to $4d\,^1\Pi_1$ and $4d\,^1\Delta_2$, which give the negative polarization ratio. By tuning the laser frequency in the wing and by measuring the polarization ratio we can partially select the different Zeeman transitions without any external magnetic or electric field. There is some analogy of this result with the case of single-photon optical collisions of polarized magnesium atoms discussed in Ref. [8]. In that paper (relating to the case of $\Delta_1 \to 0$) the similar behavior of the polarization ratio was observed in experiment and explained in the quasistatic model. However, the quasistatic theory gives a larger difference for the polarization ratio in the resonance and in the wings. Thus we can see in this example that for the light rare-gas partners the description of the fractional optical collision based on quasistatic approximation while ignoring two-photon Condon transitions and interference effects is in an accordance with the real situation only qualitatively.

V. CONCLUSION

We have analyzed by perturbation theory technique the two-photon polarization-dependent fractional optical collision. Based on the second order of a distorted wave approximation we have derived expressions for the cross sections of the fractional collision, which are valid for light with arbitrary statistical properties. In its general form the cross section is expressed as the overlap integral of its spectral profile with the spectrum of the second order correlation function of electromagnetic field.

The semiclassical expansion of both the wave functions and the retarded Green function lets us express the spectral profile of the cross section in terms of well understood semiclassical characteristics of the process. As follows from the results of Sec. III B the transition amplitudes are determined by the overlap integrals depending on such well known characteristics of classical scattering as classical actions and deflection angles calculated along the classical trajectories involved in the process. The atoms can change their trajectories of motion because of the general nonadiabatic dynamics of the atomic collision. In the semiclassical representation the polarization-dependent part of the cross section is determined by rotational transformations of the transition dipole moments and by adiabatic or nonadiabatic transition amplitudes defined along the classical trajectory. In the general case the polarization dependence of the fractional optical collision can be analyzed only numerically. However, in the quasistatic limit, determined by large frequency detunings, the polarization dependence of the two-photon absorption can be simply estimated as was discussed in Sec. III C.

In our numerical calculations we have considered the example of Mg-He ($3s^2\,^1S_0 \to 3p\,^1P_1 \to 5s\,^1S_0, 4d\,^1D_2$) fractional optical collisions. In the case of the excitation up to the $5s\,^1S_0$ state of magnesium we have obtained that for negative detuning $\Delta_1+\Delta_2$ the polarization ratio is in an accordance with its quasistatic estimation. The partial wave analysis shows the validity of the quasistatic approximation for such detunings in the general case. However, for the positive detuning $\Delta_1+\Delta_2$ we have obtained the dominant role of the contribution coming from the two-photon Franck-Condon transitions. Such a contribution can give a different magnitude of the polarization ratio than in the quasistatic model, because the two-photon Franck-Condon transitions cannot be treated as successive single-photon excitations. Specifically for the $3s^2\,^1S_0 \to 3p\,^1P_1 \to 5s\,^1S_0$ photoexcitation channel the polarization ratio for two-photon Franck-Condon transitions approaches unity. In the more complicated case of the excitation up to the $4d\,^1D_2$ state of magnesium the role of the interference between all the involved transitions becomes important and the quasistatic approximation is suitable here only qualitatively. The polarization ratio has a stable value close to $\frac{1}{7}$ in a broad range in the blue wing of the second frequency detuning. There is also a strong dependence of the polarization ratio in the red wing of the second detuning. This result can be explained by the partial selection in the wing of the atomic resonance line, perturbed by the collisions, those Zeeman atomic transitions whose contributions in the polarization ratio have different orders and different signs.

ACKNOWLEDGMENTS

We are grateful to M. Havey for stimulating and fruitful discussions. The financial support for this work was provided in part by the U.S. Civilian Research and Development Foundation (CRDF) under Grant No. RP1-263 and by the Russian Foundation for Basic Research (RFBR) under Grant No. 98-02-17719.

APPENDIX A: SEMICLASSICAL REPRESENTATION OF THE RETARDED GREEN FUNCTION

1. General analysis

The retarded Green function [kernel of retarded Green operator (2.13)] is defined as follows:

$$G^{(+)}(\mathbf{R}_2,q_2;\mathbf{R}_1,q_1) = \sum_{\Omega} \int \frac{d^3k}{(2\pi)^3} \frac{\Psi^{(+)}_{\mathbf{k}\Omega}(\mathbf{R}_2,q_2)\Psi^{(+)*}_{\mathbf{k}\Omega}(\mathbf{R}_1,q_1)}{E-E_{k\Omega}+i0} \tag{A1}$$

and it performs one of the possible solutions of the Schrödinger equation,

$$\{E-H\}G^{(+)}(\mathbf{R}_2,q_2;\mathbf{R}_1,q_1) = \delta(\mathbf{R}_2-\mathbf{R}_1)\,\delta(q_2-q_1), \tag{A2}$$

where the Hamiltonian H is applied to the first set of variables.

Making the expansion of the Green function in the adiabatic basis set with fixed total angular momentum J and projection M,

$$G^{(+)}(\mathbf{R}_2,q_2;\mathbf{R}_1,q_1)=\frac{1}{4\pi R_2R_1}\sum_{\Omega_2\Omega_1}\sum_{JM}(2J+1)\times D^{J*}_{M\Omega_2}(\alpha_2,\beta_2,0)D^{J}_{M\Omega_1}(\alpha_1,\beta_1,0)\times G^{J}_{\Omega_2\Omega_1}(R_2,R_1)\phi_{\Omega_2}(R_2,q_2)\times\phi^{*}_{\Omega_1}(R_1,q_1), \tag{A3}$$

we transform the Schrödinger equation (A2) to its radial form

$$\left\{E+\frac{\hbar^2}{2m}\frac{d^2}{dR_2^2}-U_{\Omega_2}(R_2)-\hbar^2\frac{J(J+1)-\Omega_2^2}{2mR_2^2}\right\}G^{J}_{\Omega_2\Omega_1}(R_2,R_1)-\sum_{\Omega'}(\hat{V}^{(R)}_{\Omega_2\Omega'}+V^{(C)}_{\Omega_2\Omega'})G^{J}_{\Omega'\Omega_1}(R_2,R_1)=\delta(R_2-R_1)\delta_{\Omega_2\Omega_1}, \tag{A4}$$

where nonadiabatic coupling is characterized by the following operators:

$$\hat{V}^{(R)}_{\Omega_2\Omega'}=-\frac{\hbar^2}{m}\left\langle\Omega_2\left|\frac{\partial}{\partial R_2}\right|\Omega'\right\rangle\frac{d}{dR_2}-\frac{\hbar^2}{2m}\left\langle\Omega_2\left|\frac{\partial^2}{\partial R_2^2}\right|\Omega'\right\rangle+\frac{\hbar^2}{2mR^2}\langle\Omega_2|j_\perp^2|\Omega'\rangle, \tag{A5}$$

$$V^{(C)}_{\Omega_2\Omega'}=\frac{\hbar^2}{mR_2^2}\left\{[J(J+1)-\Omega_2(\Omega_2-1)]^{1/2}\times\left\langle\Omega_2\left|\frac{1}{\sqrt{2}}j_{+1}\right|\Omega'\right\rangle-[J(J+1)-\Omega_2(\Omega_2+1)]^{1/2}\left\langle\Omega_2\left|\frac{1}{\sqrt{2}}j_{-1}\right|\Omega'\right\rangle\right\},$$

which are known as radial-type and Coriolis rotational-type nonadiabatic interactions, respectively. Here we use the following set of irreducible components of electronic angular momentum:

$$j_0=j_\zeta,\quad j_{\pm1}=\mp\frac{j_\xi\pm ij_\eta}{\sqrt{2}},\quad j_\perp^2=j_\xi^2+j_\sigma^2, \tag{A6}$$

where we assume the following directions of a Cartesian frame: ζ axis is along the $\mathbf{R}$ direction, ξ axis is along $\mathbf{R}\times\mathbf{k}$, and η axis is along $\mathbf{R}\times(\mathbf{R}\times\mathbf{k})$.

The retarded-type solution of the radial scattering equations (A5) can be found by making the appropriate choice of the boundary conditions taken from the asymptotic behavior of Eq. (A1). It can be shown that the radial Green function should satisfy the following boundary condition:

$$G^{J}_{\Omega_2\Omega_1}(R_2,R_1)\to\frac{im}{\hbar^2(k_2k_1)^{1/2}}[S^{(+)J}_{\Omega_2\Omega_1}(k_2,k_1)\times e^{ik_2R_2+ik_1R_1-i\pi J}-\delta_{\Omega_2\Omega_1}e^{ik_1(R_>-R_<)}] \tag{A7}$$

at $R_2,R_1\to\infty$ where we denoted $R_>=\max\{R_2,R_1\}$ and $R_<=\min\{R_2,R_1\}$. Here $S^{(+)J}_{\Omega_2\Omega_1}(k_2,k_1)$ is the usual S matrix of the multichannel scattering problem and k_2,k_1 are the wave numbers of initial and final states relating to the same total energy.

In semiclassical form the radial Green function can be expressed in a similar way as the radial wave functions, see Eqs. (3.15), i.e., in terms of slowly varying amplitudes and rapidly oscillating exponential functions. For a radial wave function the procedure was described in [24]. Here we briefly show how to apply it to the Green function problem. Let us make the following substitution in the scattering equations (A4):

$$G^{J}_{\Omega_2\Omega_1}(R_2,R_1)=\sum_l{}'\left\{\frac{im}{\hbar^2[k_l^J(R_2,+)k_l^J(R_1,-)]^{1/2}}g_l^J(R_2,R_1;+-)e^{i\mathcal{S}_l^J(R_2,R_1;+-)+i\pi/2}-\frac{im}{\hbar^2[k_l^J(R_2,-)k_l^J(R_1,-)]^{1/2}}g_l^J(R_2,R_1;-)e^{i\mathcal{S}_l^J(R_2,R_1;-)+i\pi/2}\theta(R_1-R_2)-\frac{im}{\hbar^2[k_l^J(R_2,+)k_l^J(R_1,+)]^{1/2}}g_l^J(R_2,R_1;+)e^{i\mathcal{S}_l^J(R_2,R_1;+)+i\pi/2}\theta(R_2-R_1)\right\}, \tag{A8}$$

where $l=\Omega_2,\Omega',\ldots,\Omega''\Omega_1$ and the prime sign indicates that the sum is expanded over all intermediate quantum numbers. Plus or minus signs in the arguments of the R-dependent wave numbers and in the transition amplitudes show the location of R_1 or R_2 points on ''out'' or ''in''parts of the classical trajectory, respectively. The action integrals are evaluated along an actual trajectory in the ''path'' potential obtained from the adiabatic potentials for each adiabatic part of atomic motion. They are given by

$$\mathcal{S}_l^J(R_2,R_1;+-)=\int_{R_l}^{R_2}k_l^J(R,+)dR+\int_{R_l}^{R_1}k_l^J(R,-)dR,$$

$$\mathcal{S}_l^J(R_2,R_1;-)=\int_{R_2}^{R_1}k_l^J(R,-)dR,$$
$$\mathcal{S}_l^J(R_2,R_1;+)=\int_{R_1}^{R_2}k_l^J(R,+)dR. \tag{A9}$$

Here R_l is the location of the turning point on the ''path'' potential $U_l(R)$. Because of θ functions in Eq. (A8) the points R_1 and R_2 are located on the classical trajectory in the preferred order in accordance with a classical picture of atomic motion.

If the radii R_1 and R_2 are close to one another and both are inside of the adiabatic region, then $g_l^J(R_2,R_1;\pm)=g^J_{\Omega_2\Omega_1}(R_2,R_1\pm)=\delta_{\Omega_2\Omega_1}$ and $g_l^J(R_2,R_1;+-)=\text{const}_{R_2,R_1}$. It is easy to see that taking into account the second order in the derivative of rapidly oscillating exponential functions and only the first order in the derivative of slowly varying factors over R_1 in Eq. (A4) one can obtain the δ function in the left side of this equation.

Consider now the situations when there is only one nonadiabatic region located between R_1 and R_2. If it is separated from the classically forbidden regions, the ''in'' and ''out'' parts of the Green function can be found independently, because they are associated with two running waves propagating via the nonadiabatic region from opposite directions. In such a case we can introduce the semiclassical form of scattering equations for slowly varying transition amplitudes $g^J_{\Omega_2\Omega_1}(R_2,R_1;\pm)$, assuming a large magnitude of angular momentum J and keeping only the derivative of these amplitudes in the first order:

$$\frac{\partial}{\partial R_2}g^J_{\Omega_2\Omega_1}(R_2,R_1;\pm)=\sum_{\Omega'}\left\{-\left(\frac{k^J_{\Omega'\Omega_1}(R_2,\pm)}{k^J_{\Omega_2\Omega_1}(R_2,\pm)}\right)^{1/2}\left\langle\phi_{\Omega_2}\left|\frac{\partial}{\partial R_2}\right|\phi_{\Omega'}\right\rangle\right.$$
$$\left.\pm\frac{i}{[k^J_{\Omega_2\Omega_1}(R_2,\pm)k^J_{\Omega'\Omega_1}(R_2,\pm)]^{1/2}}\frac{(J+1/2)}{R_2^2}\langle\phi_{\Omega_2}|j_\xi|\phi_{\Omega'}\rangle\right\}$$
$$\times\exp\{iS^J_{\Omega'\Omega_1}(R_2,R_1;\pm)-iS^J_{\Omega_2\Omega_1}(R_2,R_1;\pm)\}g^J_{\Omega'\Omega_1}(R_2,R_1;\pm). \tag{A10}$$

These equations should be considered in combination with the following boundary conditions: $g^J_{\Omega_2\Omega_1}(R_2,R_1;+)\to\delta_{\Omega_2\Omega_1}$ at $R_2\to R_1+0$ and $g^J_{\Omega_2\Omega_1}(R_2,R_1;-)\to\delta_{\Omega_2\Omega_1}$ at $R_2\to R_1-0$. It is important that by substituting the ''in'' and ''out'' terms of the Green function into scattering equation (A4) the δ function vanishes if we neglect the terms

$$\frac{J+\frac{1}{2}}{k^J_{\Omega_2}(R_2)k^J_{\Omega_1}(R_1)R^2}\langle\phi_{\Omega_2}|j_\xi|\phi_{\Omega_1}\rangle\delta(R_2-R_1),$$

where we denote $k^J_{\Omega_2}(R_2)=k^J_{\Omega_2\Omega_1}(R_2,\pm)$, $k^J_{\Omega_1}(R_1)=k^J_{\Omega_1\Omega_1}(R_1,\pm)$. Such types of terms lead to the similar correction in the solution of differential equation (A4) as other terms that are neglected, which come from higher order derivations of slowly varying amplitudes.

In the general case there are several separated nonadiabatic regions and we can express ''out'' and ''in'' amplitudes as the products of partial factors relating to each region as follows:

$$g_l^J(R_2,R_1;\pm)=g^J_{\Omega_2\Omega',\ldots,\Omega''\Omega_1}(R_2,R_1;\pm)$$
$$=g^J_{\Omega_2\Omega'}(R_2,R';\pm)\cdots g^J_{\Omega''\Omega_1}(R'',R_1;\pm), \tag{A11}$$

where $R_2>R'>\cdots>R''>R_1$ for the ''out'' wave and $R_2<R'<\cdots<R''<R_1$ for the''in'' wave. In these products the internal radii R' and R'' have an arbitrary location inside intermediate adiabatic domains and their possible variation does not change the product itself.

The ''in''-''out'' contribution in the semiclassical expansion of the Green function (A8) can also be formed as a product of partial solutions for each nonadiabatic region. In the asymptote $R_1,R_2\to\infty$ we should recover the semiclassical expansion of the S matrix in accordance with boundary condition (A7). The most difficult is to expand the solution in the vicinities of the classically forbidden regions, but in the simple situation with only one turning point R_0 we can express the amplitude $g_l^J(R_2,R_1;+-)$ as follows:

$$g_l^J(R_2,R_1;+-)=g^J_{\Omega_2\Omega',\ldots,\Omega^{IV}\Omega_1}(R_2,R_1;+-)$$
$$=g^J_{\Omega_2\Omega'}(R_2,R';+)\cdots g^J_{\Omega''\Omega_0}(R'',R_0;+)$$
$$\times g^J_{\Omega_0\Omega'''}(R_0,R''';-)\cdots g^J_{\Omega^{IV}\Omega_1}(R^{IV},R_1;-), \tag{A12}$$

where $R_2>R'>\cdots>R''>R_0$ and $R_0<R'''<\cdots<R^{IV}<R_1$ and internal radii $R',\ldots,R^{IV}$ are located inside the adiabatic domains.

2. Application to the $^1P_1$ state

Let us illustrate the general discussion of the preceding section by the practical example of a $^1P_1$ atomic state split into $^1\Sigma_0^+$ and $^1\Pi_1$ molecular states in the interaction with a rare-gas atom. There is only Coriolis (no radial) coupling as

$R \to \infty$ asymptote for these terms. We will use an approximation that Coriolis coupling is negligible inside the sphere with radius $R_d = R_d(J)$ (so-called decoupling sphere) and becomes important outside this sphere. Such a decoupling (locking) radius approximation is well known in the theory of atomic collisions and particularly in the theory of optical collisions, see [31–33]. It means that the change from *d* to *a* coupling schemes in Hund's classification takes place in a narrow domain located near the decoupling radius R_d. The optimal choice of R_d has been a subject of several discussions, see [32,33]. From a practical point of view the decoupling sphere approximation is useful so long as the long-range dynamical forces disappear at large internuclear separations more rapidly than long-range inertial Coriolis forces. To estimate the location of decoupling radius we may use the following:

$$\frac{\hbar^2(J+1/2)}{mR_d^2} \sim \Delta U(R_d), \tag{A13}$$

where we denote as $\Delta U(R)$ the splitting between the Σ and Π terms.

In such an assumption the slowly varying amplitudes can be calculated as a solution of simplified Eqs. (A10). On one hand, outside of the decoupling sphere, where both atomic potentials approach zero, we can solve these equations in a straight line trajectory approximation with strong Coriolis coupling between the Σ and Π states. On the other hand, inside the decoupling sphere we can use an adiabatic approximation with neglect of the Coriolis coupling. The decoupling sphere defines the sharp border between *d* and *a* Hund's regions where we fit the solutions. Final results depend on different relationships between total angular momentum *J*, decoupling radius R_d, and radii R_1, R_2.

Consider the optical collision with large impact parameter $\rho = (J+1/2)/k > \rho_0$ where $\rho_0 = R_d(\rho_0)$ is the upper value of impact parameter for the classical trajectory touching the decoupling sphere. That implies the scattering conditions where the trajectory is located inside the *d* coupling scheme region. There is no dynamical interaction between the atoms in Hund's case *d* region (atoms are free) and the slowly varying amplitudes are defined as rotational transformations characterizing the change in the orientation of the molecular frame for the motion along the trajectory from point R_1 to point R_2:

$$g^J_{\Omega_2\Omega_1}(R_2,R_1;-) = D^j_{\Omega_2\Omega_1}(-\pi/2, -\xi^J(R_2,R_1;-), \pi/2), \quad R_2 < R_1$$

$$g^J_{\Omega_2\Omega_1}(R_2,R_1;+) = D^j_{\Omega_2\Omega_1}(-\pi/2, -\xi^J(R_2,R_1;+), \pi/2), \quad R_2 > R_1 \tag{A14}$$

$$g^J_{\Omega_2\Omega_1}(R_2,R_1;+-) = D^j_{\Omega_2\Omega_1}(-\pi/2, -\xi^J(R_2,R_1;+-), \pi/2).$$

The Wigner *D* functions describe the rotational transformation of the atomic wave functions with internal angular momentum j ($j=1$) and they depend on deflection angles $\xi^J(R_2,R_1;\pm)$, $\xi^J(R_2,R_1;+-)$. The references of the deflection angles used here and throughout are shown in Fig. 11. We show here and below the full structure of the *l* index in the subscript of the *g* functions and omit it in deflection angles. This can be done because the deflection angles relate here to the straight parts of the classical trajectory and do not depend on *l*.

If $\rho = (J+1/2)/k < \rho_0$ and $R_2, R_1 > R_d$ then ''in'' and ''out'' parts of the trajectory between R_1 and R_2 are located inside the *d* Hund case region, but the ''in''-''out'' part crosses the *a* region. The Coriolis-type transition amplitudes are given by

$$g^J_{\Omega_2\Omega_1}(R_2,R_1;-) = D^j_{\Omega_2\Omega_1}(-\pi/2, -\xi^J(R_2,R_1;-), \pi/2), \quad R_2 < R_1$$

$$g^J_{\Omega_2\Omega_1}(R_2,R_1;+) = D^j_{\Omega_2\Omega_1}(-\pi/2, -\xi^J(R_2,R_1;+), \pi/2), \quad R_2 > R_1 \tag{A15}$$

$$g^J_{\Omega_2\Omega'\Omega_1}(R_2,R_1;+-) = D^j_{\Omega_2\Omega'}(-\pi/2, -\xi^J(R_2,R_d;+), \pi/2) \times D^j_{\Omega'\Omega_1}(-\pi/2, -\xi^J(R_d,R_1;-), \pi/2).$$

If $R_1 > R_d > R_2$ then the ''in'' and ''in''-''out'' parts of the trajectory can cross the decoupling sphere and the amplitudes are given by

$$g^J_{\Omega_2\Omega_1}(R_2,R_1;-) = D^j_{\Omega_2\Omega_1}(-\pi/2, -\xi^J(R_d,R_1;-), \pi/2),$$
$$g^J_{\Omega_2\Omega_1}(R_2,R_1;+-) = D^j_{\Omega_2\Omega_1}(-\pi/2, -\xi^J(R_d,R_1;-), \pi/2). \tag{A16}$$

If $R_2 > R_d > R_1$ then the ''out'' and ''in''-''out'' parts of the trajectory can cross the decoupling sphere and the transition amplitudes are the following:

$$g^J_{\Omega_2\Omega_1}(R_2,R_1;+) = D^j_{\Omega_2\Omega_1}(-\pi/2, -\xi^J(R_2,R_d;+), \pi/2),$$
$$g^J_{\Omega_2\Omega_1}(R_2,R_1;+-) = D^j_{\Omega_2\Omega_1}(-\pi/2, -\xi^J(R_2,R_d;+), \pi/2). \tag{A17}$$

If $R_d > R_1, R_2$ then all the parts of the trajectory are inside Hund's case *a* region and all the amplitudes are purely adiabatic,

$$g^J_{\Omega_2\Omega_1}(R_2,R_1;-) = \delta_{\Omega_2\Omega_1}, \quad R_2 < R_1$$

$$g^J_{\Omega_2\Omega_1}(R_2,R_1;+) = \delta_{\Omega_2\Omega_1}, \quad R_2 > R_1 \tag{A18}$$

$$g^J_{\Omega_2\Omega_1}(R_2,R_1;+-) = \delta_{\Omega_2\Omega_1}.$$

The last relation between R_1, R_2, and R_d is typical for optical transitions in quasistatic conditions when, in accordance with the Frank-Condon principle, the optical excitation is initiated inside the molecular interaction region.

APPENDIX B: SEMICLASSICAL REPRESENTATION OF RADIAL WAVE FUNCTION $V^{(-)}_{\Omega\Omega}(R)$ FOR THE $4d\,^1D_2$ STATE

The semiclassical representation of the radial wave function $v^{(-)}_{\Omega\Omega}(R)$ is defined by Eq. (3.15) as follows:

$$v^{(-)J}_{\Omega\Omega}(R)=\sum_l{}' \frac{i}{2\sqrt{k}}e^{-i\delta^J_l(k,+)} \times\left\{\frac{1}{[k^J_l(R,-)]^{1/2}}b^J_l(R,-)e^{-iS^J_l(R,-)-i\pi/4} -\frac{1}{[k^J_l(R,+)]^{1/2}}b^J_l(R,+)e^{iS^J_l(R,+)+i\pi/4}\right\}. \tag{B1}$$

General analysis of such kinds of semiclassical expansion as well as the details of the technique developed for calculation of slowly varying amplitudes $b^J_l(R,\pm)$ can be found in [24]. Here we present and briefly discuss only the results relating to the $4d\,^1D_2$ state of magnesium in collision with a rare-gas atom.

We restrict ourselves by considering the Coriolis nonadiabatic coupling and ignore the radial nonadiabatic interaction. As follows from the numerical results for Mg-He singlet potentials, see Fig. 4, there is no significant radial nonadiabatic coupling between Σ terms correlated with $5s$ and $4d$ electronic configurations of magnesium. The most important peculiarity of the Coriolis interaction, coming from the behavior of potentials depicted in Fig. 4, is in the existence of two decoupling spheres splitting different Hund's regions. The outer sphere, characterized by decoupling radius $R_{d1}\sim 38$ a.u., bounds the interaction region from the outer region of the free motion, which is specified as Hund's case *d*. There is an extended region located between outer sphere R_{d1} and inner sphere $R_{d2}\sim 9$ a.u., which cannot be specified in a regular Hund's classification, where only the electronic shell with $4d\sigma$ configuration has a significant repulsive interaction. The repulsive interaction comes from strong exchange interaction of $4d\sigma$ electron with the rare-gas atom. The $4d\pi$ and $4d\delta$ configurations are still degenerate at such intermediate separations because of no exchange overlapping with the wave functions of the valence electrons of the rare-gas atom and the corresponding terms are determined by zero potentials. Therefore in the rotating molecular frame there is a strong Coriolis coupling between $^1\Pi$ and $^1\Delta$ electronic states in this intermediate region. In the inner region with internuclear separations less than R_{d2} the interaction is characterized by Hund's case *a*.

For the long-range trajectories with impact parameter $\rho=(J+1/2)/k>\rho_{01}$, where $\rho_{01}=R_{d1}(\rho_{01})$ is its upper value for the limit trajectory touching the outer decoupling sphere, all the amplitudes are given by

$$b^J_l(R,+)=b^J_{\bar{\Omega}\Omega}(R,+)=D^j_{\bar{\Omega}\Omega}(-\pi/2,\xi^J(\infty,R;+),\pi/2), \tag{B2}$$

$$b^J_l(R,-)=b^J_{\bar{\Omega}\Omega}(R,-)=D^j_{\bar{\Omega}\Omega}(-\pi/2,\xi^J(\infty,R;+-),\pi/2).$$

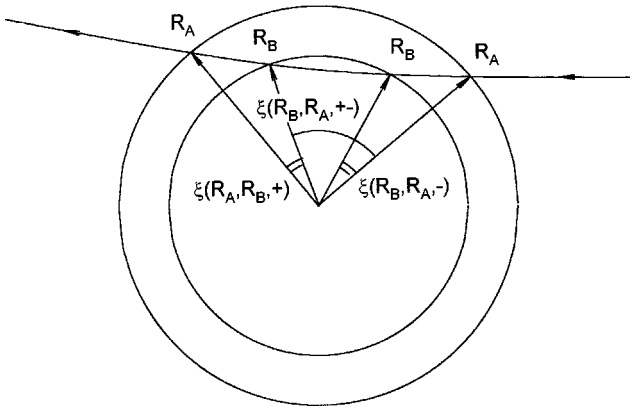

FIG. 11. The reference of the deflection angles used in the arguments of D functions in Eqs. (A14)–(A17). Here the radii R_A and R_B are any of R_1, R_2, or R_d.

Here and below we use the same reference of deflection angles as in Fig. 11.

For the intermediate trajectories with impact parameter $\rho_{02}<\rho<\rho_{01}$, where $\rho_{02}=R_{d2}(\rho_{02})$ is its upper value for the limit trajectory touching the inner decoupling sphere, the amplitudes have different representations in dependence on the relation between R and R_{d1}:

(1) ''Out'' trajectory with $R>R_{d1}$,

$$b^J_l(R,+)=b^J_{\bar{\Omega}\Omega}(R,+)=D^j_{\bar{\Omega}\Omega}(-\pi/2,\xi^J(\infty,R;+),\pi/2). \tag{B3}$$

(2) ''Out'' trajectory with $R<R_{d1}$,

$$b^J_l(R,+)=b^J_{00\Omega}(R,+)=D^j_{0\Omega}(-\pi/2,\xi^J_{d1},\pi/2),$$

$$b^J_l(R,+)=b^J_{\pm1\pm1\Omega}(R,+)=\cos\xi^J(R_{d1},R;+)\times D^j_{\pm1\Omega}(-\pi/2,\xi^J_{d1},\pi/2),$$

$$b^J_l(R,+)=b^J_{\pm1\pm2\Omega}(R,+)=-i\sin\xi^J(R_{d1},R;+)\times D^j_{\pm2\Omega}(-\pi/2,\xi^J_{d1},\pi/2), \tag{B4}$$

$$b^J_l(R,+)=b^J_{\pm2\pm2\Omega}(R,+)=\cos\xi^J(R_{d1},R;+)\times D^j_{\pm2\Omega}(-\pi/2,\xi^J_{d1},\pi/2),$$

$$b^J_l(R,+)=b^J_{\pm2\pm1\Omega}(R,+)=-i\sin\xi^J(R_{d1},R;+)\times D^j_{\pm1\Omega}(-\pi/2,\xi^J_{d1},\pi/2),$$

where $\xi^J_{d1}=\xi^J(\infty,R_{d1};+)$.

(3) ''In'' trajectory with $R<R_{d1}$,

$$b^J_l(R,-)=b^J_{00\Omega}(R,-)=D^j_{0\Omega}(-\pi/2,\xi^J_{d1},\pi/2), \tag{B5}$$

$$b^J_l(R,-)=b^J_{\pm1\pm1\Omega}(R,-)=\cos\xi^J(R_{d1},R;+-)\times D^j_{\pm1\Omega}(-\pi/2,\xi^J_{d1},\pi/2),$$

$$b^J_l(R,-)=b^J_{\pm1\pm2\Omega}(R,-)=-i\sin\xi^J(R_{d1},R;+-)\times D^j_{\pm2\Omega}(-\pi/2,\xi^J_{d1},\pi/2),$$

$$b_l^J(R,-)=b^J_{\pm 2\pm 2\Omega}(R,-)=\cos\xi^J(R_{d1},R;+-)\times D^j_{\pm 2\Omega}(-\pi/2,\xi^J_{d1},\pi/2),$$

$$b_l^J(R,-)=b^J_{\pm 2\pm 1\Omega}(R,-)=-i\sin\xi^J(R_{d1},R;+-)\times D^j_{\pm 1\Omega}(-\pi/2,\xi^J_{d1},\pi/2).$$

(4) ''In'' trajectory with $R>R_{d1}$,

$$b_l^J(R,-)=b^J_{\bar{\Omega}l'}(R,-)=D^j_{\bar{\Omega}\Omega'}(-\pi/2,\xi^J(R_{d1},R;-),\pi/2)\times b_{l'}(R_{d1},-), \tag{B6}$$

where $b_{l'}(R_{d1},-)$ is any of the amplitudes from case (3) taken at $R=R_{d1}$ and by l' in path index $l=\bar{\Omega}l'$ we denoted $l'=\Omega',\ldots,\Omega$. We do not mark the deflection angles in Eqs. (B3)–(B6) by path index because all of them relate here to the straight trajectory approximation.

For the inner trajectories with impact parameter $\rho<\rho_{02}$ the amplitudes have different representations in their dependence on the relation between R, R_{d1}, and R_{d2}.

(1) ''Out'' trajectory with $R>R_{d1}$. All the amplitudes $b_l^J(R,+)$ are given by expression (B3).

(2) ''Out'' trajectory with $R_{d1}>R>R_{d2}$. All the amplitudes $b_l^J(R,+)$ are given by expression (B4).

(3) ''Out'' and ''in'' trajectories with $R<R_{d2}$,

$$b_l^J(R,-)=b_l^J(R,+)=b_l^J(R_{d2},+). \tag{B7}$$

This region relates to the region of adiabatic evolution and $b_l^J(R_{d2},+)$ with all possible l given by Eq. (B4) at $R\to R_{d2}$.

(4) ''In'' trajectory with $R_{d1}>R>R_{d2}$,

$$b_l^J(R,-)=b^J_{000\Omega}(R,-)=D^j_{0\Omega}(-\pi/2,\xi^J_{d1},\pi/2), \tag{B8}$$

$$b_l^J(R,-)=b^J_{\pm 1\pm 1\pm 1\Omega}(R,-)=\cos\xi^J(R_{d2},R;-)\times\cos\xi^J(R_{d1}R_{d2};+)\times D^j_{\pm 1\Omega}(-\pi/2,\xi^J_{d1},\pi/2),$$

$$b_l^J(R,-)=b^J_{\pm 1\pm 2\pm 1\Omega}(R,-)=-\sin\xi^J(R_{d2},R;-)\sin\xi^J(R_{d1}R_{d2};+)\times D^j_{\pm 1\Omega}(-\pi/2,\xi^J_{d1},\pi/2),$$

$$b_l^J(R,-)=b^J_{\pm 1\pm 1\pm 2\Omega}(R,-)=-i\cos\xi^J(R_{d2},R;-)\times\sin\xi^J(R_{d1}R_{d2};+)D^j_{\pm 2\Omega}(-\pi/2,\xi^J_{d1},\pi/2),$$

$$b_l^J(R,-)=b^J_{\pm 1\pm 2\pm 2\Omega}(R,-)=-i\sin\xi^J(R_{d2},R;-)\cos\xi^J(R_{d1}R_{d2};+)\times D^j_{\pm 2\Omega}(-\pi/2,\xi^J_{d1},\pi/2),$$

$$b_l^J(R,-)=b^J_{\pm 2\pm 2\pm 2\Omega}(R,-)=\cos\xi^J(R_{d2},R;-)\cos\xi^J(R_{d1}R_{d2};+)\times D^j_{\pm 2\Omega}(-\pi/2,\xi^J_{d1},\pi/2),$$

$$b_l^J(R,-)=b^J_{\pm 2\pm 1\pm 2\Omega}(R,-)=-\sin\xi^J(R_{d2},R;-)\sin\xi^J(R_{d1}R_{d2};+)\times D^j_{\pm 2\Omega}(-\pi/2,\xi^J_{d1},\pi/2),$$

$$b_l^J(R,-)=b^J_{\pm 2\pm 2\pm 1\Omega}(R,-)=-i\cos\xi^J(R_{d2},R;-)\sin\xi^J(R_{d1}R_{d2};+)\times D^j_{\pm 1\Omega}(-\pi/2,\xi^J_{d1},\pi/2),$$

$$b_l^J(R,-)=b^J_{\pm 2\pm 1\pm 1\Omega}(R,-)=-i\sin\xi^J(R_{d2},R;-)\cos\xi^J(R_{d1}R_{d2};+)\times D^j_{\pm 1\Omega}(-\pi/2,\xi^J_{d1},\pi/2).$$

(5) ''In'' trajectory with $R>R_{d1}$,

$$b_l^J(R,-)=b^J_{\bar{\Omega}l'}(R,-)=D^j_{\bar{\Omega}\Omega'}(-\pi/2,\xi^J(R_{d1},R;-),\pi/2)b_{l'}(R_{d1},-), \tag{B9}$$

where $b_{l'}(R_{d1},-)$ is any of the amplitudes from case (4) taken at $R=R_{d1}$ and by l' in path index $l=\bar{\Omega}l'$ we denoted $l'=\Omega',\ldots,\Omega$. All the deflection angles appearing in these expressions can be calculated in zero potential, i.e., in a straight trajectory approximation.

[1] K. Burnett, Phys. Rep. **118**, 339 (1985).
[2] W. Behmenburg, V. Kroop, and F. Rebentrost, J. Phys. B **18**, 2693 (1985).
[3] D. Segal and K. Burnett, J. Phys. B **22**, 247 (1989).
[4] D. Segal and D. Harris, J. Chem. Phys. **94**, 2713 (1991).
[5] D. A. Olsgaard, M. D. Havey, and A. Sieradzan, Phys. Rev. A **43**, 6117 (1991).
[6] I. M. Bell, C. J. K. Quayle, K. Burnett, and D. M. Segal, Phys. Rev. A **47**, 3128 (1993).
[7] J. Grosser, D. Gundelfinger, A. Maetzing, and W. Behmenburg, J. Phys. B **27**, L367 (1994).
[8] R. A. Lasell, D. A. Olsgaard, M. D. Havey, and D. V. Kupriyanov, Phys. Rev. A **50**, 423 (1994); R. A. Lasell, B. S. Bayram, M. D. Havey, D. V. Kupriyanov, and S. V. Subbotin, *ibid.* **56**, 2095 (1997).
[9] J. Grosser, D. Hohmeier, and S. Klose, J. Phys. B **29**, 299 (1996); *Spectral Line Shapes*, edited by M. Zoppi and L. Ulivi, AIP Conf. Proc. No. 386 (AIP, New York, 1997), Vol. 9, p. 181.
[10] S. Yeh and P. R. Berman, Phys. Rev. A **22**, 1403 (1980).
[11] G. Alber and J. Cooper, Phys. Rev. A **31**, 3644 (1985).
[12] M. Belsley, Phys. Rev. A **42**, 6641 (1990).

[13] D. A. Olsgaard, R. A. Lasell, M. D. Havey, and A. Sieradzan, Phys. Rev. Lett. **69**, 1745 (1992); Phys. Rev. A **48**, 1987 (1993).
[14] M. Dantus, M. J. Rosker, and A. H. Zewail, J. Chem. Phys. **87**, 2395 (1987); A. H. Zewail, J. Phys. Chem. **97**, 12 427 (1993).
[15] *Femtochemistry 97*, special issue of Phys. Chem. A **102**, No. 23 (1998), edited by A. Welford Castleman and V. Sundström.
[16] O. V. Konstantinov and V. I. Perel, Zh. Eksp. Teor. Fiz. **39**, 197 (1960) [Sov. Phys. JETP **12**, 142 (1960)]; M. I. Dyakonov and V. I. Perel, *ibid.* **47**, 1483 (1964) [**20**, 997 (1965)].
[17] L. V. Keldysh, Zh. Eksp. Teor. Fiz. **47**, 1515 (1964) [Sov. Phys. JETP **20**, 1018 (1965)].
[18] E. M. Lifshitz and L. P. Pitaevskii, *Course of Theoretical Physics: Physical Kinetics* (Pergamon, Oxford, 1981).
[19] D. A. Varshalovich, A. N. Moskalev, and V. K. Khersonskii, *Quantum Theory of Angular Momentum* (World Scientific, Singapore, 1988).
[20] R. Glauber, *Optical Coherence and Photon Statistics in Quantum Optics and Electronics* (Gordon and Breach, New York, 1965).
[21] P. S. Julienne and F. H. Mies, Phys. Rev. A **30**, 831 (1984); **34**, 3792 (1986).
[22] L. L. Vahala, P. S. Julienne, and M. D. Havey, Phys. Rev. A **34**, 1856 (1986).
[23] E. E. Nikitin and S. Ya. Umanskii, *Theory of Slow Atomic Collisions* (Springer, Berlin, 1984).
[24] D. V. Kupriyanov, Chem. Phys. **193**, 141 (1995).
[25] W. Happer, Rev. Mod. Phys. **44**, 169 (1972).
[26] A. Omont, Prog. Quantum Electron. **5**, 69 (1977).
[27] The covariant B_{KQ} and contravariant B_K^Q components of arbitrary tensor B are connected as $B_K^Q=(-)^Q B_{K-Q}$.
[28] V. G. Gorbachev, D. V. Kupriyanov, I. M. Sokolov, and A. I. Trubilko (unpublished).
[29] E. Czuchaj (unpublished).
[30] L. D. Landau and E. M. Lifshits, *Quantum Mechanics* (Pergamon, Oxford, 1965).
[31] E. L. Lewis, M. Harris, W. J. Alford, J. Cooper, and K. Burnett, J. Phys. B **16**, 553 (1983).
[32] I. V. Hertel, H. Schmidt, A. Baring, and E. Meyer, Rep. Prog. Phys. **48**, 375 (1985).
[33] J. Grosser, Z. Phys. D **3**, 39 (1986).